*Journal of Applied Polymer Science*

WILEY

Applied Polymer SCIENCE

RESEARCH ARTICLE OPEN ACCESS

# Nanoparticles From Infusion Beverage Wastes and Their Effect on PLA/PHB Plasticized Composite Behavior

Jaume Sempere-Torregrosa[1] | Harrison de la Rosa-Ramírez[1] | Franco Dominici[2] | Debora Puglia[2] | Luigi Torre[2] | María Dolores Samper[1]

[1]Departamento de Ingeniería Mecánica y de Materiales (DIMM), Universitat Politècnica de València (UPV), Instituto Universitario de Tecnología de Materiales (IUTM), Alcoy (Alicante), Spain | [2]Civil and Environmental Engineering Department, University of Perugia, Terni, Italy

**Correspondence:** Jaume Sempere-Torregrosa (jausemto@epsa.upv.es)

**Received:** 3 April 2025 | **Revised:** 24 July 2025 | **Accepted:** 28 July 2025

**Funding:** This research was funded by MCIN/AEI/10.13039/501100011033 through the PID-AEI Project (grant PID2021-123753NA-C33) and the TED-AEI Project (grant TED2021-129920A-C43) and, as appropriate, by "ERDF A way of making Europe", by the "European Union" or by the "European Union NextGenerationEU/PRTR". M.D. Samper thanks the Spanish Ministerio de Ciencia, Innovacin y Universidades for the funding received for the José Castillejo mobility stay (grant CAS21/00379).

**Keywords:** corn oil | nanocomposites | nanoparticles | natural plasticizers | polyhydroxybutyrate | polylactic acid beverage waste

## ABSTRACT

In this work, yerba mate (nYM) and black tea (nBT) nanoparticles were extracted from *Ilex paraguariensis* and *Camellia sinensis*, respectively. Unlike traditional biocomposites and additives, this approach valorizes the waste of infusion beverages without using chemical compounds. Nanoparticles underwent preliminary TGA analysis, showing stable and high degradation temperature, making them suitable for processing with the selected polymer matrix. Subsequently, they were incorporated into the selected PLA (75%)–PHB (25%) blend plasticized with maleinized corn oil (MCO) at a concentration of 1–3 wt.%. Tensile characterization of the PLA-PHB blend plasticized with MCO showed an improvement in compatibility between polymers, with increased ductility. The plasticizing effect of MCO was confirmed by calorimetric analysis, showing a remarkable decrease in $T_g$ value. The combination of MCO and nanoparticles continues to exhibit enhanced thermal stability, showing functional nanofiller behavior. Moreover, the presence of nanoparticles enhanced the barrier property of the plasticized films toward oxygen barrier properties, reducing the OTR-*e* values. Finally, during the second half of the composting test, it was observed that nanoparticle addition delayed the degradation process; otherwise, it continued showing interesting biodegradable properties. These findings open multiple possibilities in the combined use of infusion beverage waste nanoparticles and modified vegetable oils to develop sustainable packaging applications.

## 1 | Introduction

Over the last decade, the demand for polymeric materials with specific characteristics across various sectors has significantly increased. Those materials are commonly considered in electronic devices manufacturing [1], food packaging and preservation, and in sectors that require non-toxic and inert materials, such as those related to the pharmaceutical industry [2].

The high demand and production rate of these materials contribute to environmental pollution, including increased $CO_2$ emissions [3] and accumulation of plastic waste, which leads to the migration of harmful chemical compounds and the release of microplastics [4].

In response to these issues, the development of more sustainable polymeric materials has increased, leading to the adoption of a

This is an open access article under the terms of the Creative Commons Attribution License, which permits use, distribution and reproduction in any medium, provided the original work is properly cited.

© 2025 The Author(s). *Journal of Applied Polymer Science* published by Wiley Periodicals LLC.

new type of polymer with lower environmental impact, known as biopolymers.

One widely studied and used biopolymer is poly-lactic acid (PLA), which is synthesized through the fermentation of corn-starch, wheat starch, and other sources [5]. PLA is a linear aliphatic polyester that is biocompatible and biodegradable, offering strength but limited ductility [6].

According to various research studies on the use of PLA in food packaging, one strategy to improve its brittleness involves blending it with other polymers. However, given the current concerns regarding petrochemical sources, biopolymers such as polybutylene adipate-co-terephthalate (PBAT) [7], polyhydroxyalkanoates (PHA) [8], or poly (ε-caprolactone) (PCL) [9] have been used to modify PLA and develop more environmentally friendly blends.

Nevertheless, the miscibility of these materials is generally low, and achieving adequate blending requires specific processing conditions. Additionally, it is important to note that PLA and PHB exhibit poor processing behavior [10], which can be influenced by the molecular weight of the added material [11, 12].

Therefore, improving the miscibility of these blends and enhancing the ductility of these systems is necessary. One approach is the use of plasticizers, which represents a more economical solution compared to copolymerization. Plasticizers, such as tar, pitch, and polymerization resins, can be of petrochemical origin. Other widely used plasticizers, such as polypropylene glycol (PPG) [13], polyethylene glycol (PEG) [14], and lactic acid oligomer (OLA) [15], are non-toxic and environmentally friendly. Plasticizing additives can also be obtained from diverse vegetable oils and fatty acids. The most commonly used plasticizers of natural origin are epoxidized palm oil (ELO) [16], epoxidized cottonseed oil (ECSO) [17], and octyl epoxy stearate (OES) [18]. Abdelwahab et al. [19] developed PLA/PHB 75/25 plasticized with polyester plasticizer (Lapol 108). In this work, the incorporation of plasticizers resulted in a homogeneous surface in the polymer matrix. A decrease in Tg values was also observed, along with an increase in elongation at break during tensile testing [19].

Another possible approach to enhance compatibility and ductility is the use of nano-additives, which are incorporated into polymeric matrices to modify and improve the properties at the nanometric level. There are different types of nano-additives from a wide variety of sources that offer valuable properties for polymeric materials.

Several studies have investigated the use of various synthetic antioxidant nanocompounds, such as butylated hydroxy anisole (BHA), butylated hydroxytoluene (BHT), and tertiary butylated hydroquinone (TBHQ), incorporated into a polypropylene (PP) matrix in film form. These films demonstrated promising properties for the development of active PP films intended for fatty food packaging [20].

Another study evaluated the incorporation of metallic nanoparticles, especially silver and copper oxide, into low-density polyethylene (LDPE) to develop active antimicrobial films aimed at increasing food safety and extending the shelf life of fresh perishable foods, such as cheese [21, 22].

In other research, nanoparticles were developed from dysprosium-cerium oxide (Dy2Ce2O7) and incorporated into biodegradable films made from wheat starch and sage seed gum (WS/SSG). These nanocomposites exhibited improvements in thermal stability, mechanical properties, UV resistance, and water barrier performance, promising results for the development of high-performance sustainable active packaging [23].

The incorporation of nanoparticles into a polymeric matrix presents a promising avenue for developing intelligent materials. For example, the study of Hossein Panahi [24] investigated the viability of single-walled carbon nanotubes (SWNTs) functionalized with iron oxide nanoparticles ($Fe_3O_4$) and coated with a biodegradable copolymer (PLA-co-mPEG) to obtain a hybrid biocompatible material capable of releasing antitumor drugs.

Another example of the effectiveness of this technology is the study conducted by Zinatloo-Ajabshir et al. [25–27] in which a magnetic nanocomposite with a hierarchical three-layer structure was developed. This nanocomposite demonstrated high efficiency results as a recyclable and stable photocatalyst, an alternative for treating contaminated water. Additional research highlights the versatility of this nanotechnology across various sectors. For instance, Rezayeenik et al. [28] developed a nanocomposite of cerium vanadate ($CeVO_4$), which was applied as a thin layer onto a copper plate heated to 100°C. The resulting material exhibited excellent electrochemical hydrogen storage capacity.

Some of these works have highlighted the potential of using renewable sources and the ease of biodegradation, making these types of additives more sustainable and resulting in a smaller carbon footprint compared to fillers derived from inorganic or petrochemical sources [29]. Research on organic waste, mostly vegetable waste, has increased to find secondary uses for such materials.

Given the high consumption of natural resources required for plastic and other compound production, it is essential to identify alternatives that reduce the use of virgin materials. The reuse of resources from the agri-food sector and post-consumer waste offers new opportunities to implement concepts such as the circular economy.

In this context, plant-based residues, such as those derived from infusion beverages, have attracted increasing attention due to their availability and inherent functional properties. For instance, Argentina is the largest producer and consumer of yerba mate (YM), which is obtained from the leaves of the *Ilex paraguariensis* tree [30]. YM has been used to obtain nanoparticles, as already reported by Arrieta et al. [31]. When added to a PLA matrix, these nanoparticles improved UV resistance, reduced UV transmission, and decreased oxygen permeability. The results also showed that incorporating nanoparticles enhanced the sustainability of PLA for potential food packaging applications [32]. Another example is black tea (BT), which comes from the leaves and buds of the *Camellia sinensis* plant. This is one of the most widely consumed teas globally, with production reaching approximately 900 000 tons annually.

Similar to YM waste, large quantities of BT waste are generated and often discarded, leading to environmental concerns. The recycling of BT waste to obtain particles was carried out by Lanjewar et al. [33], who incorporated this filler into a polypropylene matrix. BT nanoparticles contributed to enhanced mechanical properties and increased crystallinity of the composite materials.

Applying a circular economic approach, the incorporation of biomass into polymer matrices has been widely studied due to the broad range of properties that can be achieved.

In this work, the reuse of vegetable waste from infusion beverages of YM and BT, which are typically discarded after consumption, was used to obtain nanoparticles using green methodologies. These methods avoided the use of organic solvents and employed a replicable technique that offers a sustainable valorization route for underutilized by-products, with potential environmental benefits, such as the production of functional nanoparticles for incorporation into biopolymer-based films.

The selected material for enhancement was a PLA-PHB (75 wt.%/25 wt.%) blend, plasticized with 2.5 wt.% maleinized corn oil (MCO), as established in previous work. That study examined the effect of plasticizer concentration on PLA-PHB blends to determine the optimal amount and avoid exudation, which could result in the opposite of the desired effect [34].

By addressing the combined system (PLA-PHA-MCO) and incorporating YM and BT nanoparticles at a concentration of 1 and 3 wt.%, we aimed to develop a sustainable alternative film for eco-friendly packaging applications. Therefore, thermal, mechanical, oxygen barrier, and disintegration behavior under composting conditions were studied to evaluate the functional properties of the resulting material.

## 2 | Experimental Section

### 2.1 | Materials

To this work, a selected material for enhancement was chosen: a PLA-PHB (75 wt.%/25 wt.%) blend plasticized with 2.5 wt.% MCO, as established in previous research [34]. In the previous study, the results showed that a low percentage of MCO improved the interaction within the PLA-PHB (75 wt.%/25 wt.%) blend.

For the combined system (PLA-PHA-MCO), a commercial grade of biodegradable PLA, Luminy L130, was used. It was obtained from Corbion Purac (Amsterdam, Netherlands) and has a density of 1.24 g cm$^{-3}$. The polihidroxibutirato (PHB) biopolymer (Biomer P226E) was supplied by Biomer (Krailling, Germany) and is characterized by a density of 1.25 g cm$^{-3}$. The vegetable corn oil (CO) (II Nutrimento, food grade) was obtained from Probios S.p.A. (Calenzano, Italy) and was modified through a maleinization process.

The nanoparticles used as nanoreinforcements were obtained by treating collected waste products from infusions beverages of YM (*Ilex paraguariensis*) and BT (*Camellia sinensis*).

### 2.2 | Nanoparticles Extraction From Infusion Waste and Characterization

The methodology used for extracting the nanoparticles from the recovered infusion beverage waste aligns with circular economic principles and contributes to reducing the accumulation of organic waste in fields. These resources represent a valuable alternative that should be considered to support a more sustainable transition. This study employs a methodology based on green chemistry concepts, emphasizing the modification and production of materials without the use of compounds that generate harmful or toxic subproducts.

Nanoparticle extraction from BT and YM was carried out by grinding the infusion waste. Prior to the grinding, infusion waste was dried at 60°C for 24 h in a recirculating air-drying oven model D-82152 from MMM Medcenter GmbH (München, Germany). Subsequently, 6 g of each powdered infusion waste was mixed with 200 mL of distilled water under magnetic stirring at room temperature. The resulting homogeneous solution was then introduced into a triple-neck round-bottom flask (500 mL) and heated up to 100°C for 60 min using a magnetic stirring heating blanket HM02 (Labbox Labware S.L, Barcelona, Spain). To prevent the solution's evaporation, a cooling tube was placed in the center neck of the round-bottom flask. Once the solution reached room temperature, an initial filtration was performed using an Erlenmeyer flask and absorption paper (Dorsan Living filtration paper: absorbance velocity 60–55 mm/10 min, grammage 60 g/m$^2$ and thickness of 0.130 mm). To remove the solid residue, the solution was filtered again under vacuum conditions, using a Büchner funnel, Kitasato flask, and filter paper (Whatman paper: diameter 110 mm and 22 μm particle retention). Finally, the solutions were frozen and then freeze-dried under vacuum conditions (−110°C for 72 h) a Freeze/Dryer Hyper Cool HC3110. This method was also employed by Arrieta et al., who extracted nanoparticle extraction from wastes of YM.

The reproducibility of the methodology developed for nanoparticle extraction provides other researchers with the opportunity to replicate it using different types of waste and to enhance the extraction process, thereby enabling the production of more efficient and sustainable materials.

#### 2.2.1 | Transmission Electron Microscopy (TEM)

The nanoparticles were analyzed by TEM from the solution obtained after vacuum filtration. Analyses were done by using TEM equipment 120 kV JEM-1400 from JEOL Oxford.

#### 2.2.2 | Fourier Transform Infrared Spectroscopy (FTIR)

The nanoparticles were examined using total reflectance FTIR spectroscopy with a Perkin Elmer Spectrum BX instrument (Perkin-Elmer, S.L. Madrid, Spain). For the analysis, the KBr disc technique was employed, involving a mixture of potassium bromide (kBr) (purity > 99.%) for analysis, ExpertQ provided by Scharlau (99 wt.%) and nanoparticles (1 wt.%). The test was performed with a resolution of 2 cm$^{-1}$, with a range

of 4000–600 $cm^{-1}$ and each sample was scanned 15 times. The films were tested directly; results were recorded over a range of 4000–650 $cm^{-1}$ with a resolution of 4 $cm^{-1}$ and 15 scans.

## 2.3 | Preparation of Nano-Biocomposite Films

Before processing, the materials were dried at 60°C for 24 h to remove any moisture. Next, varying different amounts of nanoparticles and plasticizer were added to the initial PLA–PHB blend, as detailed in Table 1. The blends were initially mixed. Following this, the mixtures were fed into a twin co-rotating screw micro extruder (DSM Xplore 5 & 15 Micro Compounder from Xplore Instruments BV, Sittard, NL) and maintained inside for 3 min at a constant speed of 90 rpm to ensure uniformity. The temperature profile was set to 175°C, 180°C, and 185°C for all nano-biocomposites formulations.

Subsequently, the nano-biocomposites were directly cast filmed using a Film Device (Xplore Instruments BV, Sittard, NL) coupled to the extruder. The winding speed for all formulations was 600 mm/min. The resulting films were approximately 60 mm wide and between 40 and 70 μm thick.

The techniques employed replicate industrial processes on a smaller scale for the development of packaging products, offering a scalable methodology but using more sustainable materials with a low carbon footprint.

## 2.4 | Film Characterization

### 2.4.1 | Mechanical Characterization

Tensile properties were determined according to the ISO 527 standard using a Lloyd Instruments LR 30K universal testing machine (Segensworth West, Foreham, UK). The test was performed by using 150 × 10 $mm^2$ rectangular samples. At least five samples were tested using a 50 N load cell. The tested speed was 10 mm $min^{-1}$, at room temperature. The tensile strength, elongation at break, and Young's modulus values were derived from the experimental results.

**TABLE 1** | Matrices and nanobiocomposites formulations.

| Matrices | PLA (wt.%) | PHB (wt.%) | MCO (wt.%) |
|---|---|---|---|
| PLA | 100 | — | — |
| PLA-PHB[a] | 75 | 25 | — |
| B-MCO | 75 | 25 | 2.5 |
| **Nano-biocomposites** | **B-MCO (wt.%)** | **nBT (wt.%)** | **nYM (wt.%)** |
| B-MCO-1nBT | 99 | 1 | — |
| B-MCO-3nBT | 97 | 3 | — |
| B-MCO-1nYM | 99 | — | 1 |
| B-MCO-3nYM | 97 | — | 3 |

[a]The PLA/PHB blend in a 75/25 wt.% ratio was called matrix B.

### 2.4.2 | Thermal Properties

To evaluate the effect of nanoparticles on the thermal transitions of the initial blend, the materials were analyzed by using a differential scanning calorimeter (DSC). The thermal analysis was carried out on the DSC25 Discovery Series differential scanning calorimeter from TA Instruments (New Castle DE, USA).

The sample weights ranged from 5 to 6 mg, and the thermal analysis was conducted in four steps: (i) dynamic heating from 30°C to 180°C, (ii) an isothermal hold at 180°C for 2 min, (iii) cooling from 180°C to −50°C, and (iv) a second dynamic heating cycle from −50°C to 290°C, all at a heating rate of 10°C/min in a nitrogen atmosphere, with a nitrogen flow rate of 66 mL/min. Statistical significance of the differences in calorimetric data was assessed under the same conditions applied for data analysis, using one-way analysis of variance (ANOVA) with OriginPro 2018 software at a 95% confidence level.

Thermal stability was assessed using thermogravimetric analysis (TGA) with a Seiko Exstar 6300 equipment from TA Instruments (New Castle, USA). Approximately 10 mg of each sample was subjected to a heating program from 30°C to 600°C at a rate of 10°C/min, under a constant nitrogen flow of 250 mL/min. The nanoparticles were analyzed using the same heating program with sample weights of approximately 3 mg.

### 2.4.3 | Static Water Contact-Angle Measurements

The goniometry test was performed using an EasyDrop Standard goniometer, model FM140 (Krüss GmdH, Hamburg, Germany) equipped with a camera to capture images of water drops on the surface of the samples. The images were analyzed using Drop Shape Analysis software (SW21; DSA1). The samples, in film form, were tested by applying drops of distilled water using a micro syringe, with volumes ranging from 2 to 6 μL. The contact angle was measured at 0, 15, and 30 s after applying the water drop, followed by five additional measurements under the same condition. This procedure was repeated in triplicate at random positions on the sample surface.

### 2.4.4 | Oxygen Transition Rate (OTR)

The OTR was measured using an oxygen permeation analyzer from Systech Instruments—Model 8000 (Metrotec S.A, Spain) under controlled specific conditions of temperature (23°C ± 1°C) and humidity, at a pressure of 2.5 atm. The films were placed inside a diffusion chamber with a constant flow of pure oxygen (99.9% purity). The volumetric flow rate of oxygen per unit area of film and unit time (OTR, $cm^3 m^{-2} day^{-1}$) was continuously monitored until a steady state was reached. The permeability coefficient, which depends on the film thickness, is proportional to OTR**e* (where *e* is thickness in mm). The oxygen barrier properties of all the films were evaluated by comparing their OTR**e* values.

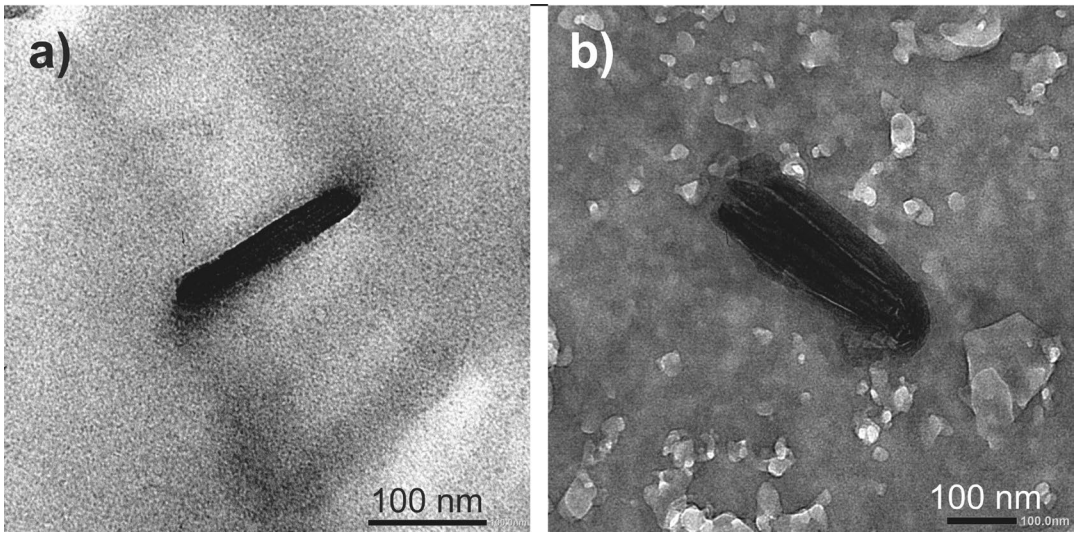



**FIGURE 1** | Images of (a) nYM and (b) nBT to ×100.

#### 2.4.5 | Water Vapor Transmission Rate (WVTR)

In the WVTR test, samples were prepared with a diameter of 63.75 mm and thickness within the range specified in the standard. The films were placed in sample capsules containing 2 mg of silica gel per sample (previously dried at 200°C for 24 h). The capsules, including the silica gel and the test film, were weighed, with the initial weight recorded as zero. The samples were placed in a temperature-controlled humidity chamber HCP (Memmert GmbH Co. KG, Schwabach, Germany) under constant conditions of 90% humidity and 23°C. The weighing process was repeated for the following 8 h, and measurements were also taken 24 h after the test began. Finally, the slope was calculated in accordance with ASTM E96/E96M–16 standards. Three samples were prepared for each formulation.

#### 2.4.6 | Microscopic Characterization

The morphology of the formulations was analyzed using Field Emission Scanning Electron Microscopy (FESEM) with a ZEISS ULTRA microscope from Oxford Instruments (Oxfordshire, UK) at an accelerating voltage of 1.5 KV. The samples were cryo-fractured prior to observation and coated with a gold–palladium alloy layer using a Sputter Mod Coater Emitech SC7620 from Quorum Technologies (East Sussex, UK) to ensure electrical conductivity.

#### 2.4.7 | Disintegration Under Composting Conditions

The disintegration test under composting conditions was conducted in accordance with the ISO 20200 standard. Film samples, cut into 25×25 mm fragments, were buried at a depth of 6 cm in plastic reactor containers and stored in an oven at a constant temperature of 58°C. Ten samples from each formulation were measured and extracted at 7, 9, 11, 14, 16, 18, 21, 25, and 30 days of the test. After extraction and prior to weighing, the recovered samples were washed with distilled water and dried for 24 h at 60°C.

The degree of disintegration ($D$) was calculated in percentage with the following Equation (1):

$$D = \frac{m_i - m_r}{m_i} \quad (1)$$

where $m_i$ is the initial dry mass of the test material, and $m_r$ is the dry mass of the residual test material recovered from the compost.

## 3 | Results and Discussion

### 3.1 | Nanoparticle Characterization

#### 3.1.1 | TEM of Nanoparticle

Figure 1 shows TEM images of nYM (Figure 1a) and nBT (Figure 1b), where the particles are observed to be on the nanometer scale: this nYM particle has dimensions of 162×28 nm, while the nBT particle shows dimensions of approximately 164×57 nm. The average size of the nYM and nBT nanoparticles was found to have values respectively of 94±6 nm and of 167±6 nm [32, 35]. Images obtained were compared with others from other works; Arrieta et al. and Beltrán et al. obtained similar structures on TEM analysis after developing similar extraction methodology using YM waste, showing long particles and slim geometry [31, 32]. Nanoparticles from BT show similar structures; otherwise, they have different sizes. Other works obtained different structures from BT waste due to the different methodologies employed and compound composition [33, 36, 37].

#### 3.1.2 | Thermogravimetric Analysis of Nanoparticles

Figure 2 and Table 2 show the TG profiles of the obtained nanoparticles and the waste material used for their production. All samples lose between 6.5% and 8.9% of moisture before reaching 96°C. The onset of the second degradation stage, marked by

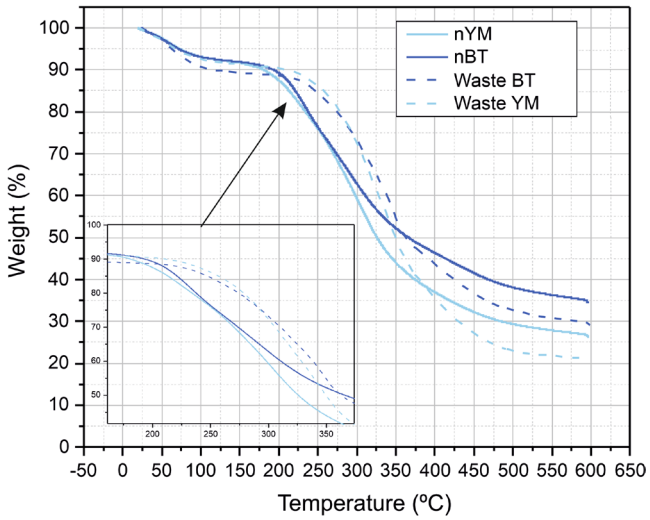



**FIGURE 2** | TGA curves of nanoparticles and infusion waste (heating rate 10°C/min, nitrogen flow rate 250 mL/min). [Color figure can be viewed at wileyonlinelibrary.com]

**TABLE 2** | TGA properties of nanoparticles and infusion waste.

| | TGA parameters | | |
|---|---|---|---|
| **Samples** | $T_{5\%}$ (°C) | $T_{max}$ (°C) | $W_{600°C}$ (%) |
| nBT | 71.7 | 233.1 | 34.4 |
| nYM | 72.7 | 303.9 | 26.1 |
| Waste BT | 63.1 | 350.3 | 29.1 |
| Waste YM | 67.4 | 344.8 | 20.5 |

the beginning of the degradation of pectin and hemicellulose, occurs in all samples above 190°C, with the degradation of the residues occurring approximately 40°C higher. However, the fact that the obtained nanoparticles degrade at lower temperatures than their corresponding residues is not a concern, as the onset degradation temperature is not reached during processing. In this temperature range, the thermal degradation of cellulose and lignin decomposition also begins, resulting in a greater mass loss around 350°C. The percentage of residual weight at 600°C ($W_{600°C}$) is higher for the nanoparticles than for the infusion waste from which they were obtained, with differences observed between both plant extracts. At 600°C, most of the organic compounds have decomposed and volatilized, leaving behind a residue of inorganic compounds, primarily oxides formed from the original minerals present in the samples. This residue is referred to as ash. The results indicate that nanoparticles obtained from BT have a higher concentration of minerals than those originating from YM, resulting in greater thermal stability. This thermal degradation is typical of lignocellulosic structures [38–44].

#### 3.1.3 | FTIR Analysis

Figure 3 represents the spectra of nanoparticles and waste from infusion beverages obtained in the first zone, ranging from 4000 to 2600 $cm^{-1}$. It can be observed that the bands of the two types of nanoparticles are similar, showing a broad band corresponding to hydroxyl groups (OH) around 3350 $cm^{-1}$, as well as asymmetric and symmetric C—H stretching vibrations around 2920 and 2850 $cm^{-1}$ (Figure 3a).

In the spectral region between 2200 and 600 $cm^{-1}$, a band appears between 1500 and 1800 $cm^{-1}$, which is attributed to the carbonyl groups of esters, amides, and acids present in the various types of nanoparticles. In the regions from 1500 to 1250 $cm^{-1}$ and from 1300 to 1000 $cm^{-1}$, scissoring vibration of $CH_3$ and $CH_2$ groups and stretching vibration of C—O bonds, respectively, were identified [31, 45–47] (Figure 3b).

In Figure 3c, for BT waste, the region of 4000–2600 $cm^{-1}$ shows a band attributed to the stretching of O-H groups between 3500 and3300 $cm^{-1}$, and another between 2900 and 2800 $cm^{-1}$ due to the vibration of aliphatic saturated C—H bonds [47, 48]. The results for YM waste are similar, but vibrations are caused by different compounds: the 3500–3300 $cm^{-1}$ band is assigned to the stretching vibration of —OH groups in cellulose and lignin molecules, while the 2900–2800 $cm^{-1}$ band is due to the stretching vibration of CH alkyl groups in the aliphatic bonds of cellulose, lignin, and hemicellulose [49].

In the region from 2200 to 600 $cm^{-1}$ (Figure 3d), BT waste shows a vibration at 1600 and 1700 $cm^{-1}$, assigned to C═O stretching of aldehyde, ketone, or carboxylic acids present in hemicellulose, with more pronounced peaks in nBT results (Figure 3b). A weaker vibration around 1550 $cm^{-1}$ is related to the aromatic C═C skeleton vibration of lignin. The vibrations between 1100 and 1000 $cm^{-1}$ result from C—O bending and stretching modes [47, 50].

For YM, a vibration band between 1610 and 1740 $cm^{-1}$ corresponds to asymmetric carbonyl stretching of ester carboxylate groups. Additionally, weak aromatic C—H vibrations are observed between 1100 and 1000 $cm^{-1}$ [49]. Finally, a similar vibration is observed around 660 and 3750 $cm^{-1}$ for both types of waste, characteristic of water and moisture content in the biomass [51].

### 3.2 | Film Characterization

#### 3.2.1 | Mechanical Properties

The results from tensile characterization of PLA samples are typically of brittle polymers, showing low elongation at break percentage and high tensile strength and Young's modulus values. The incorporation of 25% of PHB shows values like those obtained in other works, affecting the behavior of the PLA matrix. Specifically, tensile strength and Young's modulus values decreased, while elongation at break increased significantly, more than double compared to neat PLA [52].

The addition of MCO as a plasticizer improved the compatibility between PLA and PHB biopolymers. Tensile strength and Young's modulus increased due to the compatibilizing effect of MCO. Furthermore, elongation at break increases significantly, reaching over 700% compared to neat PLA [53–55]. These results suggest that the designated B formulation experiences a compatibilizing effect through the incorporation of

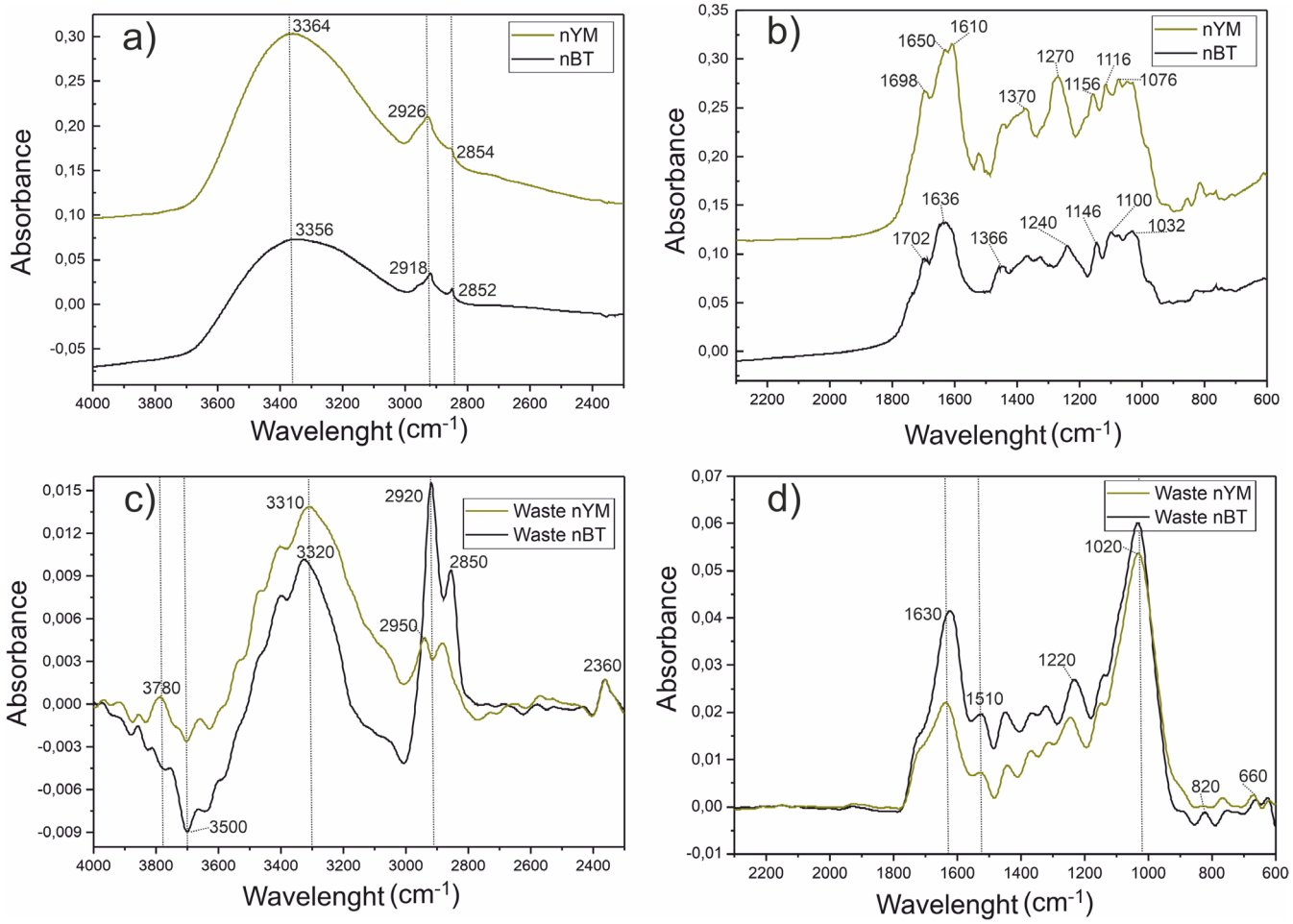



**FIGURE 3** | FTIR of nanoparticles and corresponding waste material, (a) nanoparticles in region from 4000 to 2600 ($cm^{-1}$) and (b) region from 2200 to 600 ($cm^{-1}$), (c) waste materails in the region from 4000 to 2600 ($cm^{-1}$) and (d) region 2200 to 600 ($cm^{-1}$) (resolution 2 $cm^{-1}$, range 4000–600 $cm^{-1}$), scans. [Color figure can be viewed at wileyonlinelibrary.com]

MCO into the matrix, reducing the number of double bonds and overall interactions between polymer chains [56, 57], thereby enhancing the miscibility of biopolymers. The changes in mechanical properties may indicate the stabilization of the matrix due to improved interfacial interaction across the phases [58, 59].

In general, the incorporation of nanoparticles causes a decrease in mechanical properties compared with the plasticized sample. The tensile strength and Young's modulus values were similar to those previously measured for neat PLA-PHB, while elongation at break, in most cases, exceeded the values observed for the blend. This behavior may be ascribed to poor dispersion of nanoparticles within the matrix. Nanoparticles present can act as stress concentration zones [60–62].

The incorporation of nBT reduces the mechanical properties to a greater extent, presenting similar tensile strength and Young's modulus values as those of the PLA-PHB sample, 28.5 and 28.7 MPa for tensile strength, and between 1950 and 2140 MPa for Young's modulus. The elongation at break also shows similar values; for instance, with 1 wt.% of nBT it is 27.6%. However, when the nBT nanoparticles increased to 3 wt.%, the elongation at break decreased to 18%. This suggests that increasing the nBT content to 3 wt.% leads to a reduction in all mechanical properties, likely due to the excess nanometric filler causing poor dispersion, stress concentration points, and delamination at the interface between the particles and plasticized matrix. For both formulations with 3 wt.%, a reduction in mechanical performance is observed, which may correspond to reaching the dispersion limit of many nanosized particles [63, 64].

In contrast, the reduction in mechanical properties for nYM is not as pronounced as for nBT. The B-MCO-1nYM, which contains nanoparticles, shows the best mechanical properties: tensile strength of 32.6 MPa, a Young's modulus of 2158 MPa, and an elongation at break of 39.2%. This represents an increase of more than 250% in elongation at break compared to neat PLA and about 50% compared to the PLA-PHB blend.

Finally, interaction between the plasticizer and the additives can be affected by the maleic anhydride content of MCO, hydroxyl groups of the lignocellulosic filler chains, and the PLA can react, leading to reactions such as linear chain extension, branching, and formation of cross-linked structures [65, 66]. The increased chain mobility provided by plasticizer may be affected by the incorporation of nanoparticles, resulting in nanocomposites, obtaining a reduction of mobility after the interaction with

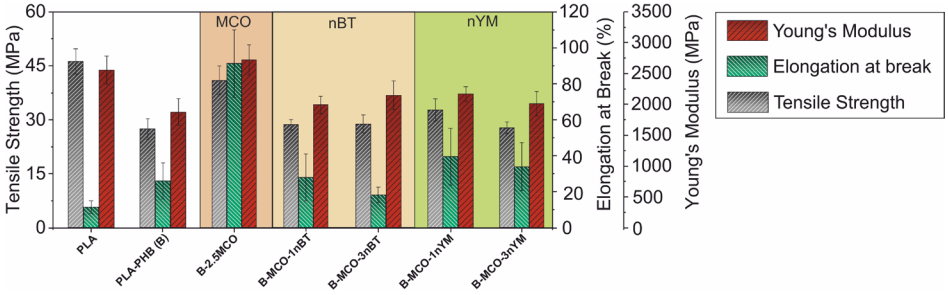



**FIGURE 4** | Principal mechanical properties of developed films (load cell 50 N, speed 10 mm $min^{-1}$). [Color figure can be viewed at wileyonlinelibrary.com]

**TABLE 3** | TGA result for developed samples.

| Samples | TGA parameters | | |
|---|---|---|---|
| | $T_{5\%}$ (°C) | $T_{max\ I}$ (°C) | $T_{max\ II}$ (°C) |
| PLA | 310.4 | — | 355.8 |
| PHB | 266.7 | 294.6 | — |
| PLA-PHB (B) | 267.9 | 281.3 | 342.7 |
| B-2.5MCO | 268.6 | 280.8 | 347.3 |
| B-M-1nBT | 267.4 | 280.5 | 342.9 |
| B-M-3nBT | 270.5 | 266.2 | 331.4 |
| B-M-1nYM | 269.1 | 280.3 | 349.3 |
| B-M-3nYM | 271.0 | 277.3 | 332.2 |

PLA's chains. These effects can lead to a decrease in mechanical performance, depending on the dispersion of the nanoparticles within the polymeric matrix. Therefore, achieving a positive interaction between the plasticizer and the nanoparticles is essential (Figure 4).

### 3.2.2 | Thermal Properties

The effect of nanoparticles on the thermal stability of the initial blend has been analyzed through a dynamic TGA measurement, and the corresponding values are represented in Table 3. It was observed that neat PLA is the sample with the highest thermal stability, beginning degradation ($T_{5\%}$) at 310.4°C. The other samples show the onset of degradation between 266°C and 271°C, which is attributed to the incorporation of PHB into the formulation, as PHB begins to degrade at 266.7°C, approximately.

Additionally, all biocomposites exhibit a two-stage degradation pattern: the first stage corresponds to PHB degradation, and the second to mass loss mainly due to PLA degradation (Figure 5a) [41]. The MCO incorporation results in a slight reduction in the onset of thermal degradation. The plasticizer leads to some thermal stability due to the increased polymer chain mobility, though this does not compromise processing.

Furthermore, nanoparticles slightly delay the onset of degradation (Figure 5b,c, and Table 3) by approximately 1°C to 2°C. However, they also caused a decrease in the $T_{max}$, advancing the degradation of both PHB (Tmax I) and PLA (Tmax II) to lower temperatures, around 15°C lower in the sample with 3 wt.% of nanoparticles. Despite this, formulations with nanoparticles show an overall increment in thermal stability, with a slightly delayed thermal degradation. This interaction between incorporated components exhibits a synergistic effect, contributing to improving the material processing.

Comparing the results with similar methodologies used in other works, TGA curves show parallel behavior a fast initial degradation to 5% of mass, followed by thermal degradation delayed after nanoparticles incorporation [32, 67]. In this studies YM derived from compounds were used, no BT studies were found, but after TEM analysis it is noticed that similar nanoparticles were obtained following same methodology for both infusion beverages. Therefore, it can be interpreted that the extracted compounds obtained similar results on TGA analysis.

Table 4 and Figure 6 show the thermograms and specific thermal transitions observed during the second heating stage performed by DSC of the samples. It is noted that the neat PLA and PHB samples exhibit the characteristic thermal transitions of their respective polymers. PLA shows a glass transition temperature ($T_g$) at 60.2°C, an exothermic process associated with a cold crystallization peak at 101.7°C, and the endothermic melting peak at 172.8°C.

For the PLA-PHB blend, the $T_g$ of PHB is observed at −4.3°C and PLA at 53.1°C [68–70] indicating that the two polymers are immiscible [12, 71].

The cold crystallization temperature ($T_{cc}$) associated with PLA shifts forward by approximately 5°C (97.5°C), and the enthalpy decreases, likely due to a nucleating effect from PHB crystals that promotes PLA crystallinity during cooling [12]. The melting process of the PLA-PHB blend appears as a single endothermic peak at 171.3°C, as the melting temperatures of both polymers are close and cannot be distinguished separately in the blend.

The addition of 2.5% MCO to the initial blend reduces the $T_g$ to 50°C, demonstrating its role as a plasticizer by increasing chain mobility [72]. Nevertheless, the observed increase in Young's Modulus, as discussed in the mechanical properties section, suggests that MCO also acts as a compatibilizer as well, enhancing miscibility within the polymer blend. This dual behavior highlights the complex role of MCO in the

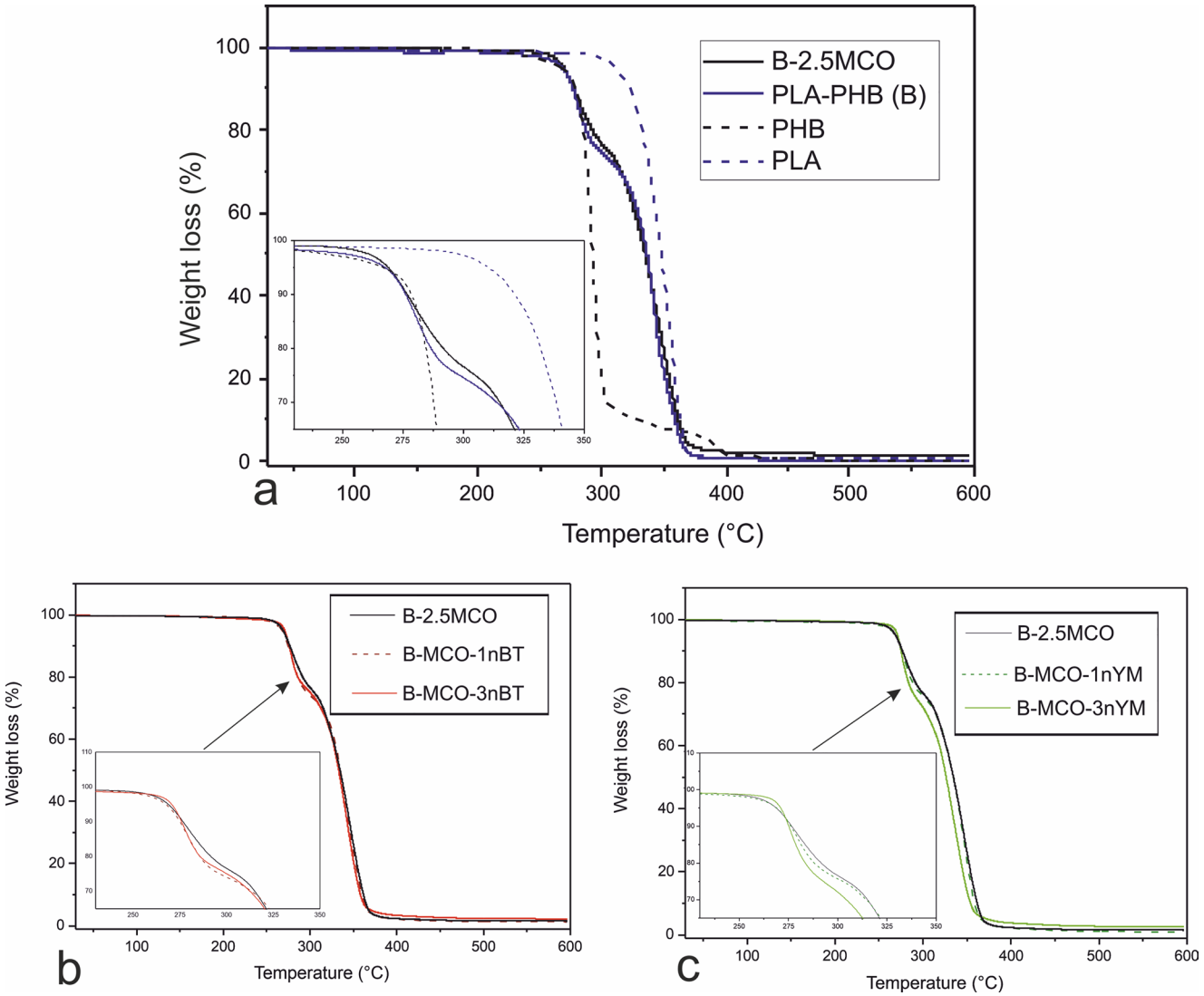



**FIGURE 5** | TGA curves of initial blends and materials (a), formulations with nBT wt.% nanoparticles and 2.5 MCO biocomposite (b), and formulations with nYM wt.% nanoparticles and 2.5 MCO biocomposite (c) (heating rate 10°C/min, nitrogen flow rate 250 mL/min). [Color figure can be viewed at wileyonlinelibrary.com]

**TABLE 4** | DSC thermal properties.

| | DSC parameters | | | | | |
|---|---|---|---|---|---|---|
| **Samples** | $T_{gPLA}$(C) | $T_{gPHB}$(C) | $T_{cc}$ (°C) | $\Delta H_{cc}$ (J/g) | $T_m$ (°C) | $\Delta H_m$ (J/g) |
| PLA | $60.2 \pm 0.5^{a}$ | — | $101.7 \pm 0.2^{a}$ | $26.3 \pm 0.4^{a}$ | $172.8 \pm 0.1^{a}$ | $57.2 \pm 1.1^{a}$ |
| PLA-PHB (B) | $53.1 \pm 0.2^{b,d}$ | $-4.3 \pm 0.3^{a}$ | $97.5 \pm 0.4^{b}$ | $10.1 \pm 1.3^{b}$ | $171.3 \pm 0.0^{b,c}$ | $43.1 \pm 1.4^{b}$ |
| B-2.5MCO | $50.0 \pm 1.0^{b,c}$ | $-3.6 \pm 0.5^{a}$ | $97.3 \pm 0.2^{b}$ | $15.3 \pm 1.0^{c}$ | $171.2 \pm 0.3^{b,c}$ | $42.8 \pm 0.8^{b}$ |
| B-M-1nBT | $48.8 \pm 0.7^{c}$ | $-3.2 \pm 0.1^{a}$ | $97.6 \pm 0.1^{b}$ | $15.2 \pm 0.5^{c}$ | $170.9 \pm 0.2^{b}$ | $40.1 \pm 1.5^{b,c}$ |
| B-M-3nBT | $54.1 \pm 0.8^{d}$ | $-3.4 \pm 0.6^{a}$ | $98.2 \pm 0.2^{b,d}$ | $15.4 \pm 1.7^{c}$ | $171.2 \pm 0.2^{b}$ | $40.4 \pm 1.2^{b,c}$ |
| B-M-1nYM | $53.1 \pm 2.6^{b,d}$ | $-4.1 \pm 0.4^{a}$ | $99.8 \pm 1.1^{c}$ | $12.6 \pm 1.1^{b,c}$ | $171.5 \pm 0.15^{b,c}$ | $39.2 \pm 1.2^{c}$ |
| B-M-3nYM | $49.3 \pm 1.3^{c}$ | $-3.3 \pm 0.5^{a}$ | $99.2 \pm 0.3^{c,d}$ | $13.5 \pm 3.9^{b,c}$ | $171.4 \pm 0.2^{b,c}$ | $39.8 \pm 1.3^{b,c}$ |

*Note:* Distinct letters (a–d) assigned to the same property, as determined by DSC, denote statistically significant differences between formulations ($p < 0.05$).

blend. The cold crystallization temperature further decreases to 97.3°C, likely due to the lubricating effect produced by the MCO [73].

The incorporation of different nanoparticles also causes a reduction in $T_g$ values for both polymers, with the effect being more pronounced when using nBT nanoparticles. Additionally,

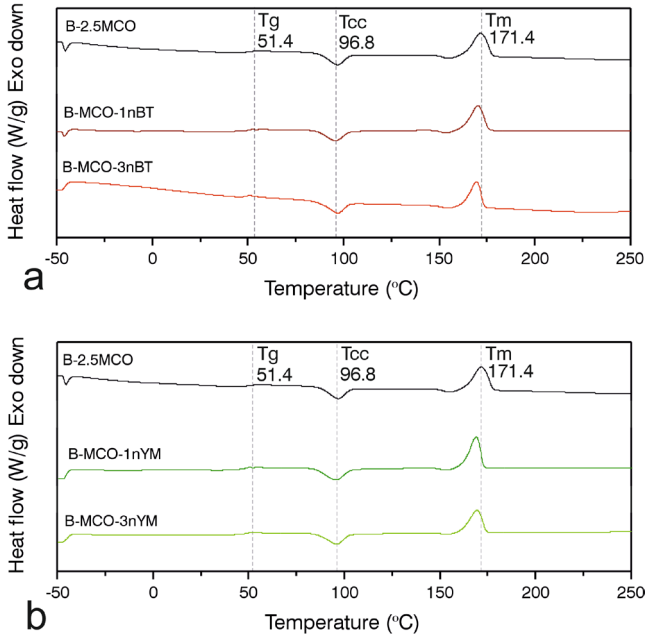



**FIGURE 6** | Calorimetric graphs of formulated materials (a) formulations with nBT and (b) formulations with nYM (heating rate 10°C/min, nitrogen flow rate 60 mL/min). [Color figure can be viewed at wileyonlinelibrary.com]

both the $T_{cc}$ and the melting temperature ($T_m$) slightly decrease with nanoparticle addition, particularly with nBT. The lowest thermal transition values are observed in the sample containing 1 wt.% of nBT, which shows a $T_g$ (associated with PLA) of 48.8°C, a $T_{cc}$ of 97.6°C, and a $T_m$ of 170.9°C. These changes suggest that nanoparticles enhance the plasticizing effect induced by the MCO.

However, as verified in the mechanical properties analysis, the addition of nanoparticles generally reduces mechanical strength and ductility compared to the B-2.5MCO sample. Still, it is worth noting that the sample with 1 wt.% nBT exhibits better mechanical performance than the PLA-PHB blends without nanoparticles.

The variation in thermal behavior and properties among formulations with different types of nanoparticles is minimal, with similar values observed due to the comparable nature of the lignocellulosic nanoparticles used. Notably, nYM achieved a higher enthalpy value associated with cold crystallization. The interaction between MCO and different kinds of nanoparticles does not significantly affect the primary thermal properties, indicating thermal stability during the heating cycle. Similar thermal results were noticed in a previous study, reducing principal thermal properties that suggest interaction with polymer chains [32].

### 3.2.3 | Static Water Contact Angle Measuring

The water contact angle test was used to estimate changes in the surface properties of formulated materials after incorporating nanoparticles. As shown in Table 5, PLA exhibits a typical water contact angle of approximately 71°. In the initial blend (B-blend), a slight increment of the contact angle of about 5° was observed at both recorded times. However, when MCO and nanoparticles were incorporated, the water contact angle decreased to a minimum of about 68°, compared to the initial blend. This reduction was more noticeable in the formulations with a higher nanoparticle content.

**TABLE 5** | Values of water contact angle measured during tests at 15 and 30 s.

| Samples | CA (°) after 15 s | CA (°) after 30 s |
|---|---|---|
| PLA | 73.3 ± 5.1 | 70.9 ± 4.2 |
| PLA-PHB (B) | 77.2 ± 3.4 | 76.9 ± 3.3 |
| B-2.5MCO | 71.6 ± 3.1 | 71.3 ± 2.9 |
| B-MCO-1nBT | 70.6 ± 3.4 | 70.4 ± 3.4 |
| B-MCO-3nBT | 69.9 ± 1.0 | 69.8 ± 1.1 |
| B-MCO-1nYM | 71.4 ± 2.0 | 71.1 ± 2.2 |
| B-MCO-3nYM | 68.2 ± 0.8 | 67.9 ± 0.8 |

Therefore, it is considered that the nanoparticles increase the surface energy, promoting better wetting and resulting in lower contact angles. According to Jose and Alagar, the surface can form strong bonds, providing a considerable energetic incentive for water to disrupt bulk bonding and interact with the material surface [74]. Moreover, it was observed that the greater the amount of nanoparticles, the higher the hydrophilic character of the material surface. This could be ascribed to the action of the nanoparticles in increasing the internal forces within the material, thereby raising the surface energy and allowing water to spread more easily on the surface. The interaction between the different added compounds suggests good interaction and facilitates the exposure of functional groups on the film surface. The results achieved in the water contact angle show an interesting result in packaging applications, and comparing these results with another work, the combination between MCO and nanoparticles obtained a great change on the topographical surface [31].

### 3.2.4 | OTR

Table 6 shows the OTR and normalized OTR values (OTR-*e*, normalized to 1 mm thickness) for the formulated material containing 1 wt.% nanoparticles, PLA, and the initial formulation (B-blend). The lower OTR-*e* values observed in the initial formulation indicate reduced oxygen permeability compared to that of neat PLA. This could be attributed to PHB acting as a nucleating agent for PLA [75], resulting in increased crystallinity, which in turn reduces the diffusion of oxygen molecules [53, 76]. The incorporation of PHB improved the oxygen barrier properties by 38.7% compared to the neat PLA sample.

As expected, with the incorporation of MCO (B-2.5MCO), the gas barrier performance of the plasticized films decreased compared to the initial blend, showing only a 29.5% improvement. This behavior is ascribed to the MCO molecules becoming intercalated between individual polymer chains, increasing free

**TABLE 6** | OTR values.

| Samples | OTR ($cm^3 m^2 day^{-1}$) | *e* (μm) | OTR-*e* ($cm^3 \cdot mm \cdot m^{-2} \cdot day^{-1}$) |
|---|---|---|---|
| PLA | 412 | 42 | 17.3 |
| PLA-PHB (B) | 303 | 35 | 10.6 |
| B-2.5MCO | 271 | 45 | 12.2 |
| B-MCO-1nBT | 162 | 52 | 8.4 |
| B-MCO-3nBT | 563 | 17 | 9.5 |
| B-MCO-1nYM | 220 | 52 | 11.4 |
| B-MCO-3nYM | 383 | 41 | 15.7 |

volume and thus facilitating oxygen diffusion [77]. Furthermore, the presence of 1 wt.% nanoparticles improved the barrier properties of plasticized films, reducing OTR-*e* values of the B-2.5MCO sample by 31% and 7%, respectively. When comparing the OTR-*e* values of samples containing 1 wt.% nanoparticles with the neat PLA sample, oxygen barrier properties improved by 51.4% and 34.1%, respectively. At 3 wt.% nanoparticle content, the OTR-*e* values increased, indicating a reduction in oxygen barrier properties. This decrease is likely due to the formation of non-uniformities, including nanoparticle agglomerates and cavities by defects, which create preferential pathways for oxygen diffusion.

Overall, the results indicate that nBT nanoparticles demonstrated higher performance as a potential oxygen barrier compared to nYM. According to Iiyas et al. [78], one of the main reasons nanocellulose can block the passage of oxygen molecules is that their kinetic diameter is on the same order as the pore size of the nanocellulose network, causing oxygen molecules to become partially trapped. In this study, the nanoparticles were of similar size, and nBT was more effective than nYM in restricting the passage of oxygen through the film. Increasing the nanoparticle content to 3 wt.% led to the formation of defects and agglomerates, which decreased the barrier effectiveness [53].

### 3.2.5 | WVTR

Compared with the initial blend, it was observed (Figure 7) that the incorporation of PHB and MCO drastically reduced the WVTR values. Materials added to the matrix can act as physical impermeable barriers and obstruct the movement of water molecules, extending the diffusion path length and enhancing water barrier properties. Incorporation of 1 wt.% resulted in lower WVTR values than the neat PLA sample. The addition of 3 wt.% of nanoparticles led to the highest WVTR values, highlighting that the formulation with 3 wt.% of nYM reached 348 g day/$m^2$.

This increase may be attributed to a more porous structure, which facilitates the water vapor transmission and reduces permeability [79, 80]. The increased porosity could be due to poor nanoparticle dispersion within the polymer matrix. Because of their inherent tendency to agglomerate, nanoparticles can create microdefects in the film, which in turn facilitates molecule transmission. While MCO incorporation increases the free

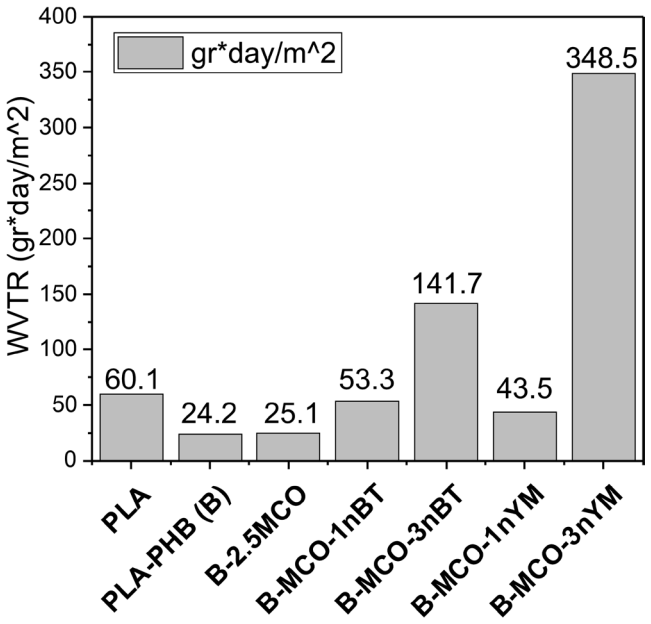



**FIGURE 7** | WVTR results of formulations (humidity 90%, temperature 23°C).

volume, well-dispersed nanoparticles can fill voids and limit pathways for vapor passage. However, poor dispersion leads to higher WVTR values and negatively affects the film surface. Similar results were noticed by Bumbudsanpharoke et al. [81] where the incorporation of nanoparticles into films obtained a decrease in barrier properties and identified the need to increase the diffusion of it in the polymeric matrix to enhance films' permeability.

### 3.2.6 | FTIR for Films

In Figure 8, an intensity peak can be observed at 2900–3000 $cm^{-1}$, corresponding to the absorption of the cyclohexene group. This overlaps with the characteristic broad —CH absorption peaks of PLA and PHB [82–84]. The FTIR curves also display an intensity peak at 1760–1750 $cm^{-1}$, consistent with findings reported by other authors and identified as the asymmetric stretching of the carbonyl group (C═O), attributed to the lactide unit in PLA.

Samples with 25% PHB content obtained curves with peak vibration at the intensities between 1740 and 1710 $cm^{-1}$

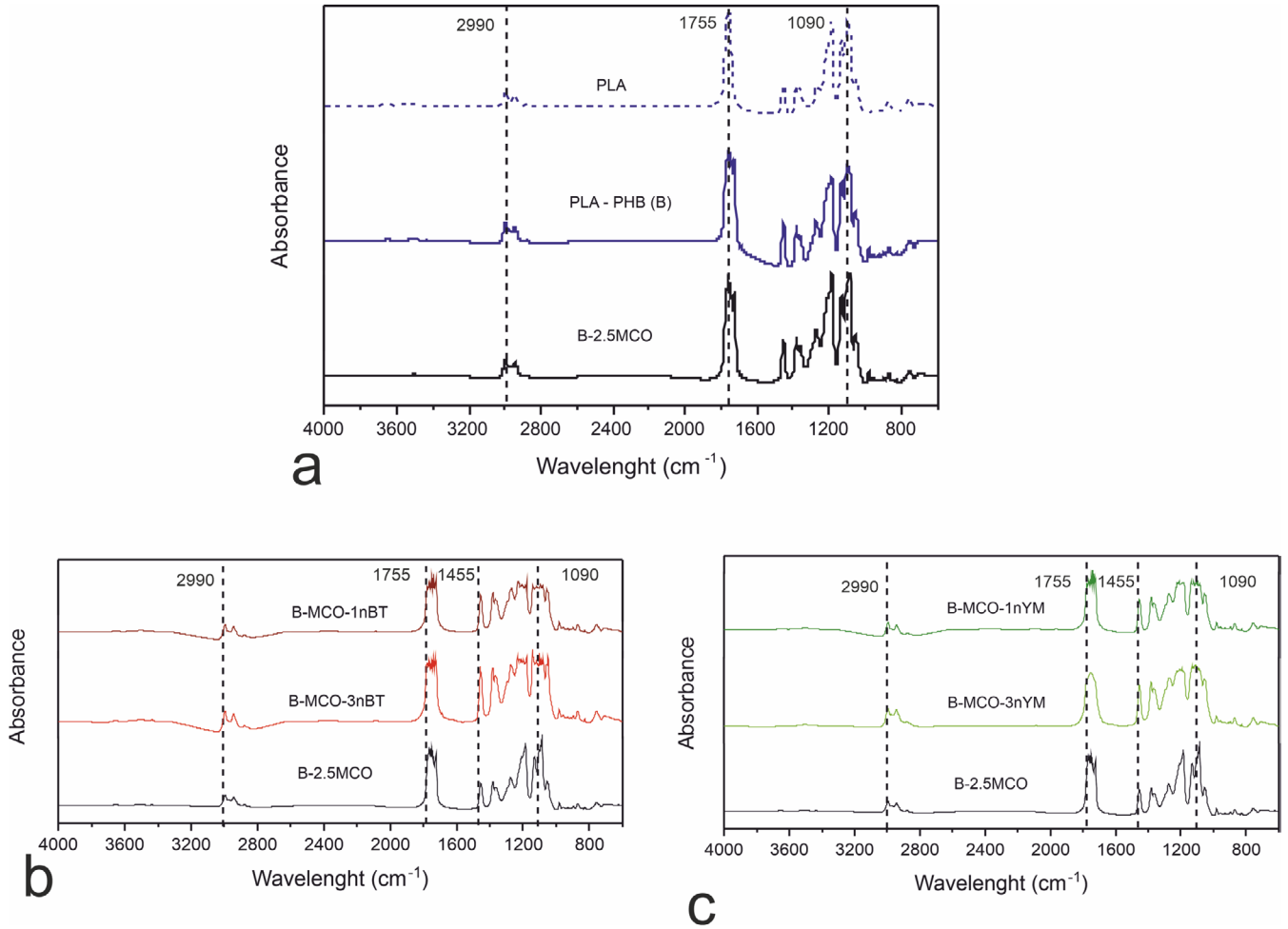



**FIGURE 8** | FTIR spectrum the initial films blends (a), formulations with plasticizer and nBT wt.% nanoparticles composites (b), and formulations with plasticizer and nYM wt.% nanoparticles composites (c) (resolution 4 $cm^{-1}$, range 4000–650 $cm^{-1}$, scans 15). [Color figure can be viewed at wileyonlinelibrary.com]

characteristic vibration of crystalline carbonyl groups C═O and amorphous carbonyl vibration of PHB, respectively [85, 86]. Vibration at 1450 $cm^{-1}$ band observed is associated with $CH_3$ group. The region of symmetric peak deformation bands corresponds to —CH, appeared at 1380 $cm^{-1}$ and asymmetric peak deformation bands at 1360 $cm^{-1}$ of PHB. According to the PHB structure, a vibration band is found at 1220 $cm^{-1}$ corresponding to the C—O—C stretching in the crystalline region, and another at 1260 $cm^{-1}$ attributed to C—O—C stretching in the amorphous region. In addition, the C—O stretching band of the —CH—O- group at 1180 $cm^{-1}$ nearly disappears. The region between 1000 and 800 $cm^{-1}$ shows deformation vibration of ═CH groups [87–89].

The FTIR spectrum of the sample containing MCO exhibits a C—H vibration band at 2990 $cm^{-1}$, attributed to aliphatic functional groups, with an increase in band intensity. Similarly, upon incorporation of MCO, a broadening of the carbonyl (C═O) bands at 1755 $cm^{-1}$ is observed, possibly indicating the formation of an extended hydrogen-bonding network between MCO and the matrix. In the same region, a slight shift toward higher frequencies is noted, which may be due to increased chemical rigidity resulting from MCO interactions. Additionally, increased band intensity is observed for the 1755 $cm^{-1}$ carbonyl bands and for the ester (C—O—C) groups located between 1450 and 1000 $cm^{-1}$. These changes may be attributed to the formation of new interactions or enhanced molecular mobility. The observed shifts and intensity changes in the MCO-related bands suggest that MCO acts both as a plasticizer and a compatibilizer. These findings are supported by the DSC curves, although these effects were questioned after the increase in Young's Modulus observed in tensile tests.

The incorporation of nBT led to an increase in band intensities, with higher nanoparticle content resulting in greater intensity. This may indicate chemical alterations and enhanced interactions between nanoparticles and the matrix. Additionally, an increase in band intensity is observed, potentially reflecting the formation of a hydrogen-bonding network between the blend components. Band shifts toward lower frequencies are also noted, which could result from a reduction in bond energy due to attractive interactions or the formation of an extended hydrogen-bonding network, as previously observed [90, 91].

For nYM, an increase in both band intensity and width is observed compared to the initial blend. However, these nanoparticles exhibit lower band intensities than the nBT formulations,

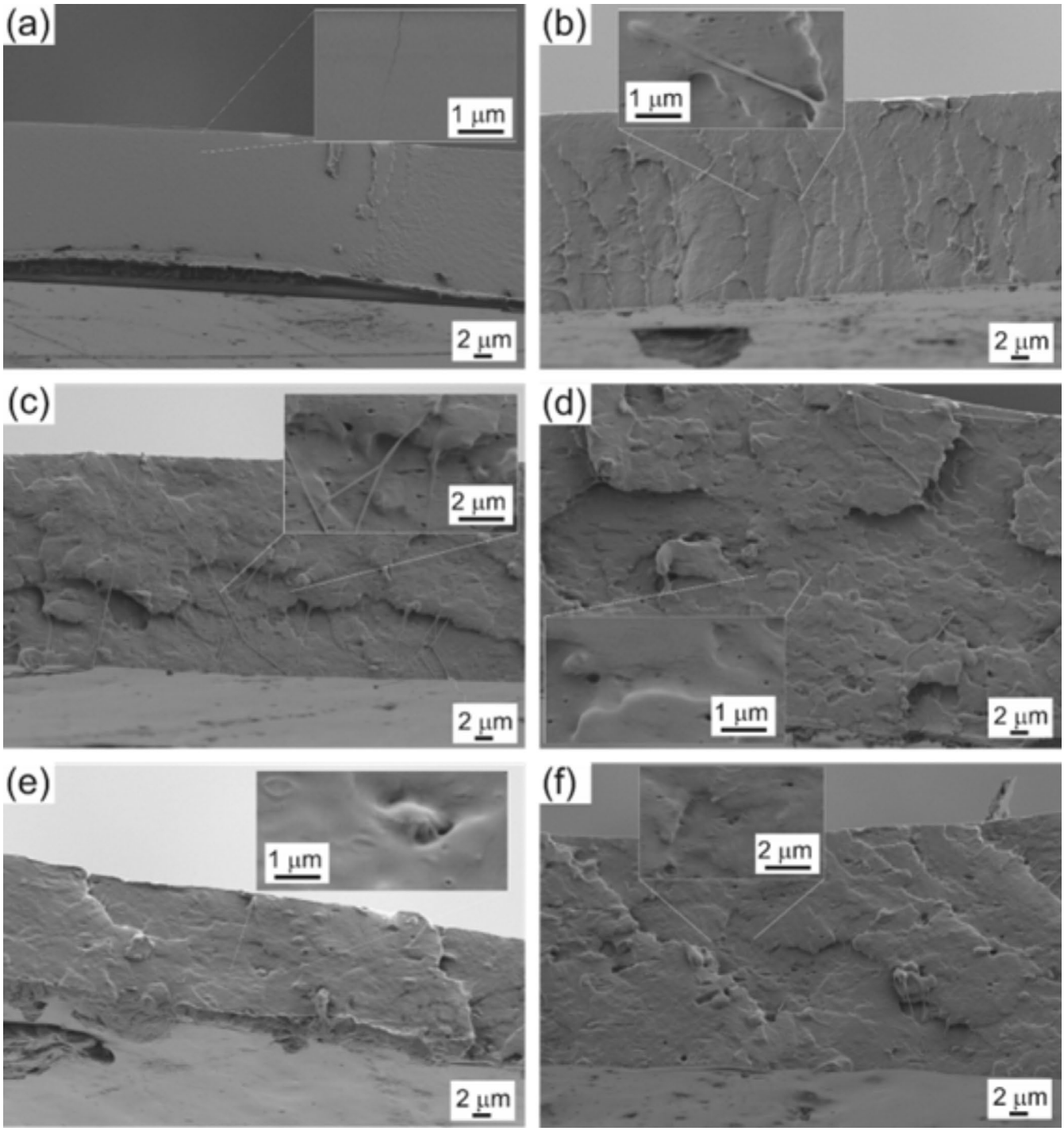



**FIGURE 9** | FESEM images of the cryofracture of films at different magnifications: (a) Neat PLA, (b) B-2.5MCO, (c) B-MCO-1nYM, (d) B-MCO-3nYM, (e) B-MCO-1nBT, and (f) B-MCO-3nBT (Voltage 1.5 KV).

as well as slight variations among formulations with different nanoparticle concentrations. This could be attributed to weaker interactions and reduced hydrogen-bond formation. The difference between formulations could be due to the variations in the composition and the size of nanoparticles. It is worth noting that the increased intensity and bandwidth of carbonyl (C═O) groups in PLA could be influenced by the carboxylic acid (—COOH) groups present in the vegetal residues, leading to band shifts toward lower frequencies and enhanced interactions among the two components [92, 93].

#### 3.2.7 | Field Emission Scanning Electron Microscopy (FESEM)

The PLA FESEM image (Figure 9a) exhibits a smooth and uniform surface, typical of brittle polymers. The incorporation of PHB and 2.5 wt.% of MCO (Figure 9b) induces a rougher surface with shallow craters. The addition of nYM further increases the surface cavities (Figure 9c,d). In contrast, the incorporation of nBT leads to a significant decrease in the number of cavities compared to the other formulations, especially those

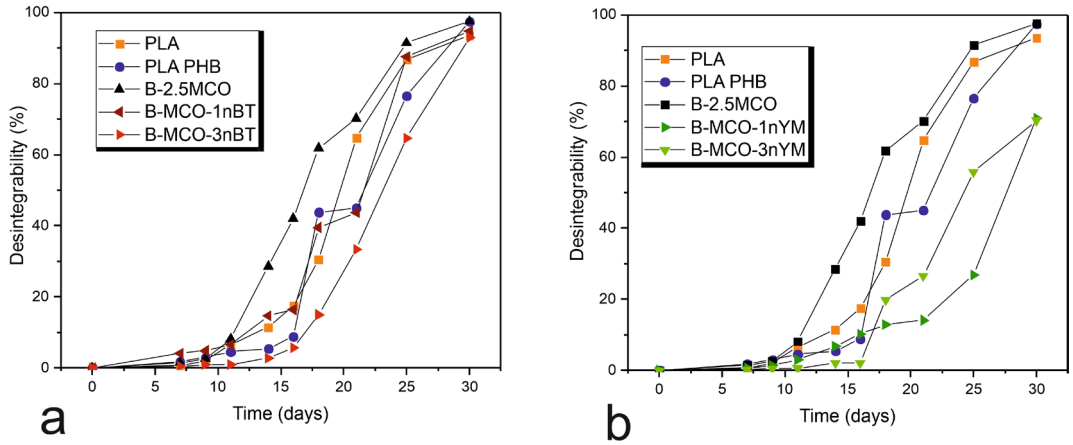



**FIGURE 10** | Evolution of the mass, in percentage, of the samples as a function of composting time of (a) initial materials and with nBT nanoparticles, (b) initial materials and with nYM nanoparticles (incubation temperature 58°C). [Color figure can be viewed at wileyonlinelibrary.com]

containing nYM (Figure 9e,f). This morphological change may be reflected in the mechanical properties (Table 3) as the nBT formulations show a greater reduction in properties, including elongation at break. This could be attributed to nanoparticle aggregation, which reduces chain mobility and acts like stress concentration points. This behavior becomes more pronounced as the nanoparticle concentration in the polymer matrix increases. The changes in the samples fracture surface were identified by other authors, observing similar rough morphology and increase of cavities after nanoparticles incorporation [31, 94, 95].

### 3.2.8 | Disintegration Under Composting Conditions

Mass variation during aerobic degradation related to formulated materials was evaluated and compared with the initial blend when different wt.% of nanoparticles were added. As expected, all samples (Figure 10) showed a loss of transparency on Day 7 of the test due to the breakage of PLA chemical bonds caused by the water molecules [96, 97]. The visual appearance of samples (Figure 11) and the degree of disintegrability indicate that, during the initial days, only fragmentation of the films and changes in hue were observed.

Also, no significant mass loss was observed in the first 10 days. However, by Day 14, a progressive increase in degradation was observed, particularly in the plasticized formulation (B-2.5MCO), which exhibited over 30% mass loss, while the remaining samples showed a degree of disintegration below 20% on the same day. The addition of PHB delayed the degradation process of PLA, mainly due to an increase in PLA crystallinity induced by the PHB. It is well known that PLA disintegration begins in amorphous regions. Moreover, the addition of nanoparticles caused an even greater delay in the degradation of the formulated materials between the first and second week. For instance, on day 18, PLA exhibited 50% disintegration, whereas formulations containing nBT showed disintegration percentages of approximately 40% and 15% for 1 nBT and 3 nBT, respectively. In the case of nYM, the samples reached 14% and 25% of disintegration on the same day for 1 nYM and 3 nYM, respectively.

On day 25, PLA and formulations with nBT overpassed 90% of disintegration (currently considered the target of disintegrability percentage according to ISO 20200 standards); meanwhile, formulations with nYM reached this target after day 30. It is known that enzymatic oxidation plays a key role in tea processing; therefore, the levels of oxidation and fermentation determine tea quality [98]. In this case, the greater delay in disintegration of the formulated materials with nYM, compared to those with nBT, could be associated with the higher concentration of antioxidant components in nYM, which results from fully fermented leaves, as compared to nBT [98, 99]. The delay observed in the second half of the composting test may be due to the good interaction between the added materials, which contributed to a compact matrix that reduces water penetration. While MCO promotes initial chain mobility, the incorporation of nanoparticles counterbalances this effect by reinforcing the matrix. This behavior is similar to that observed in the OTR test, suggesting on one hand that small samples have fewer microspheres on the surface and on the other hand highlighting the need to achieve better nanoparticle dispersion to reduce the permeability values. Nevertheless, the disintegrability values under composting conditions meet the requirements for sustainable materials.

The slower degradation observed in the second half of the test after the incorporation of nanoparticles can be considered beneficial from an environmental standpoint, depending on the type of application and the intended life cycle of the product. In one scenario, a delayed disintegration in the final stages may help preserve the material's structural integrity, as long as biodegradation is eventually achieved in compliance with regulatory standards, avoiding accumulation of plastic residues. In a second scenario, for single-use applications, a higher degree of disintegration may be preferable. Therefore, the observed behavior is considered acceptable, as the delay in the degradation rate under composting conditions complies with the criteria of the standard used to classify a polymer material as biodegradable.

## 4 | Conclusions

The extraction process of nanoparticles from infusion beverage waste was successful and aligned with the concept of the circular economy and waste minimization. Utilizing residues as raw

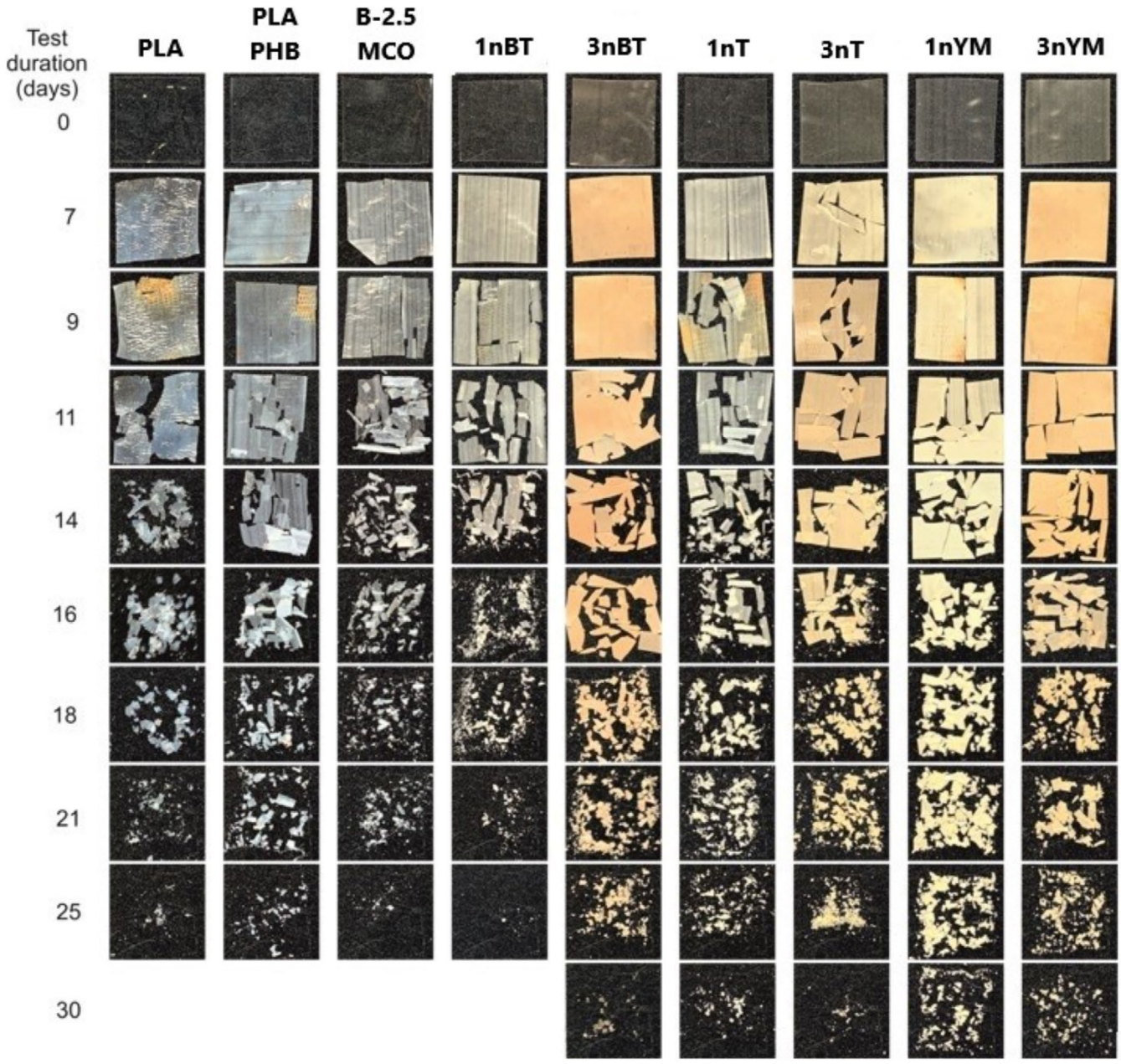



**FIGURE 11** | Visual images of samples analyzed in disintegration under composting conditions (incubation temperature 58°C). [Color figure can be viewed at wileyonlinelibrary.com]

materials contributes to sustainability by replacing the use and synthesis of petroleum-based additives. Furthermore, the methodology employed adheres to key principles of green chemistry, avoiding the use and generation of toxic compounds, and is easily replicable for various organic waste materials.

Thermal characterization showed that nanoparticle incorporation slightly delays the onset of degradation temperature. However, the $T_{max}$ values exhibit a smaller shift, with a higher decrease observed at 3 wt.% of nanoparticle content. The DSC results reveal molecular interactions between the compounds, such as the decrease in $T_g$ due to the plasticizing effect of MCO, and a reduction in the main thermal transitions, promoting improved ductility in the nanoparticles-containing formulation. The combination of MCO and nanoparticles results in enhanced thermal stability, allowing for possible processing.

The molecular interactions of these nano-biocomposites were also analyzed using FTIR, which indicated improved interfacial interactions and enhanced compatibility between phases. Although this interaction is expected to improve mechanical properties, the incorporation of nanoparticles led to a partial reduction of the ductility improvement provided by the plasticizer. This behavior could be attributed to the limited dispersion of nanoparticles; however, formulations containing nanoparticles still achieve more ductile properties compared to the initial PLA-PHB blend.

Moreover, nanoparticle-containing formulations showed an increase in WVTR values, likely due to poor dispersion of the nanoparticles, which tend to agglomerate. This behavior may result in micropore formation by nature, facilitating the transmission of water molecules. Nevertheless, the nanoparticles

demonstrated high performance as potential oxygen barriers, an essential property for a functional packaging material.

Surface analysis using FESEM revealed a transition from a smooth surface to one with visible cavities. Under composting conditions, the disintegration of the nano-biocomposites was delayed by approximately 1 week compared to the control blend. This suggests that the nano-biocomposites developed a more resistant structure against microbial attack, reaffirming the potential barrier properties against water penetration.

Development of these materials generates a positive environmental impact by utilizing nanocomposites to reduce the amount of virgin material used and repurposing waste to create biodegradable materials that facilitate the ecological transition. This approach reduces the use of petrochemical-based polymers and additives while minimizing plastic waste generation.

The characterization results suggest that the developed materials could serve as an alternative to pure PLA and other biopolymers in food packaging applications where controlled permeability is required, such as packaging for fruits and vegetables that benefit from respiration and moisture exchange. To further enhance the performance of these materials, improvements in nanoparticle dispersion prior to processing are recommended, such as using ultrasound to blend nanoparticles with the plasticizer. Overall, this study proposes a sustainable and innovative approach to improving the functional and environmental performance of biodegradable packaging materials through the valorization of post-infusion biomass.

### Author Contributions

**Jaume Sempere-Torregrosa:** formal analysis (equal), investigation (equal). **Harrison de la Rosa-Ramírez:** formal analysis (equal), validation (equal). **Franco Dominici:** investigation (equal), methodology (equal), writing – review and editing (equal). **Debora Puglia:** methodology (equal), writing – review and editing (equal). **Luigi Torre:** supervision (equal). **María Dolores Samper:** conceptualization (lead), funding acquisition (lead), investigation (lead), project administration (lead), writing – review and editing (lead).


### Acknowledgments

This research was funded by MCIN/AEI/10.13039/501100011033 through the PID-AEI Project (grant PID2021-123753NA-C33) and the TED-AEI Project (grant TED2021-129920A-C43) and, as appropriate, by "ERDF A way of making Europe", by the "European Union" or by the "European Union NextGenerationEU/PRTR". M.D. Samper thanks the Spanish Ministry of Science, Innovation and Universities for the funding received for the José Castillejo mobility stay (grant CAS21/00379). H. de la Rosa-Ramírez thanks Universitat Politècnica de València for his post-doctoral PAID-10-24 grant.


### Conflicts of Interest

The authors declare no conflicts of interest.

### Data Availability Statement

The data that support the findings of this study are available from the corresponding author upon reasonable request.

### References


1. C. Dingler, K. Dirnberger, and S. Ludwigs, "Semiconducting Polymer Spherulites—From Fundamentals to Polymer Electronics," *Macromolecular Rapid Communications* 40, no. 1 (2019): 1800601, https://doi.org/10.1002/MARC.201800601.

2. T. Aziz, A. Ullah, A. Ali, et al., "Manufactures of Bio-Degradable and Bio-Based Polymers for Bio-Materials in the Pharmaceutical Field," *Journal of Applied Polymer Science* 139 (2022): e52624, https://doi.org/10.1002/app.52624.

3. F. M. Baena-Moreno, E. le Saché, L. Pastor-Pérez, and T. R. Reina, "Membrane-Based Technologies for Biogas Upgrading: A Review," *Environmental Chemistry Letters* 18, no. 5 (2020): 1649–1658, https://doi.org/10.1007/S10311-020-01036-3/TABLES/6.

4. C. Bollaín, C. Bollaín Pastor, and D. V. Agulló, "Colaboración Especial," 2019, www.msc.es/resp.

5. M. Jamshidian, E. A. Tehrany, M. Imran, M. Jacquot, and S. Desobry, "Poly-Lactic Acid: Production, Applications, Nanocomposites, and Release Studies," *Comprehensive Reviews in Food Science and Food Safety* 9, no. 5 (2010): 552–571, https://doi.org/10.1111/J.1541-4337.2010.00126.X.

6. J. I. Fajardo, L. E. Valarezo, L. M. López, and A. P. Sarmiento, "Experiencies in Obtaining Polymeric Composites Reinforced With Natural Fiber From Ecuador," *Ingenius* 9 (2013): 28–35, https://doi.org/10.17163/INGS.N9.2013.04.

7. N. T. Kilic, B. N. Can, M. Kodal, and G. Ozkoc, "Compatibilization of PLA/PBAT Blends by Using Epoxy-POSS," *Journal of Applied Polymer Science* 136, no. 12 (2019): 47217, https://doi.org/10.1002/APP.47217.

8. M. L. Iglesias Montes, V. P. Cyras, L. B. Manfredi, V. Pettarín, and L. A. Fasce, "Fracture Evaluation of Plasticized Polylactic Acid / Poly (3-HYDROXYBUTYRATE) Blends for Commodities Replacement in Packaging Applications," *Polymer Testing* 84 (2020): 106375, https://doi.org/10.1016/J.POLYMERTESTING.2020.106375.

9. R. U. Rao, B. Venkatanarayana, and K. N. S. Suman, "Enhancement of Mechanical Properties of PLA/PCL (80/20) Blend by Reinforcing With MMT Nanoclay," *Materials Today: Proceedings* 18 (2019): 85–97, https://doi.org/10.1016/J.MATPR.2019.06.280.

10. J. W. Park, Y. Doi, and T. Iwata, "Uniaxial Drawing and Mechanical Properties of Poly[(R)-3-Hydroxybutyrate]/Poly(L-Lactic Acid) Blends," *Biomacromolecules* 5, no. 4 (2004): 1557–1566, https://doi.org/10.1021/BM049905L.

11. N. Koyama and Y. Doi, "Miscibility of Binary Blends of Poly[(R)-3-Hydroxybutyric Acid] and Poly[(S)-Lactic Acid]," *Polymer (Guildf)* 38, no. 7 (1997): 1589–1593, https://doi.org/10.1016/S0032-3861(96)00685-4.

12. M. Zhang and N. L. Thomas, "Blending Polylactic Acid With Polyhydroxybutyrate: The Effect on Thermal, Mechanical, and Biodegradation Properties," *Advances in Polymer Technology* 30, no. 2 (2011): 67–79, https://doi.org/10.1002/ADV.20235.

13. E. Piorkowska, Z. Kulinski, A. Galeski, and R. Masirek, "Plasticization of Semicrystalline Poly(l-Lactide) With Poly(Propylene Glycol)," *Polymer (Guildford)* 47, no. 20 (2006): 7178–7188, https://doi.org/10.1016/J.POLYMER.2006.03.115.

14. W. Ke, X. Li, M. Miao, B. Liu, X. Zhang, and T. Liu, "Fabrication and Properties of Electrospun and Electrosprayed Polyethylene Glycol/Polylactic Acid (PEG/PLA) Films," *Coatings* 11, no. 7 (2021): 790, https://doi.org/10.3390/COATINGS11070790.

15. N. Burgos, V. P. Martino, and A. Jiménez, "Characterization and Ageing Study of Poly(Lactic Acid) Films Plasticized With Oligomeric Lactic Acid," *Polymer Degradation and Stability* 98, no. 2 (2013): 651–658, https://doi.org/10.1016/J.POLYMDEGRADSTAB.2012.11.009.

16. F. Dominici, M. D. Samper, A. Carbonell-Verdu, et al., "Improved Toughness in Lignin/Natural Fiber Composites Plasticized With

Epoxidized and Maleinized Linseed Oils," *Materials* 13, no. 3 (2020): 600, https://doi.org/10.3390/ma13030600.

17. A. Carbonell-Verdu, M. D. Samper, D. Garcia-Garcia, L. Sanchez-Nacher, and R. Balart, "Plasticization Effect of Epoxidized Cottonseed Oil (ECSO) on Poly(Lactic Acid)," *Industrial Crops and Products* 104 (2017): 278–286, https://doi.org/10.1016/j.indcrop.2017.04.050.

18. D. Garcia-Garcia, A. Carbonell-Verdu, M. P. Arrieta, J. López-Martínez, and M. D. Samper, "Improvement of PLA Film Ductility by Plasticization With Epoxidized Karanja Oil," *Polymer Degradation and Stability* 179 (2020): 109259, https://doi.org/10.1016/J.POLYMDEGRADSTAB.2020.109259.

19. M. A. Abdelwahab, A. Flynn, B. Sen Chiou, S. Imam, W. Orts, and E. Chiellini, "Thermal, Mechanical and Morphological Characterization of Plasticized PLA–PHB Blends," *Polymer Degradation and Stability* 97, no. 9 (2012): 1822–1828, https://doi.org/10.1016/J.POLYMDEGRADSTAB.2012.05.036.

20. S. H. Fasihnia, S. H. Peighambardoust, S. J. Peighambardoust, A. Oromiehie, M. Soltanzadeh, and D. Peressini, "Migration Analysis, Antioxidant, and Mechanical Characterization of Polypropylene-Based Active Food Packaging Films Loaded With BHA, BHT, and TBHQ," *Journal of Food Science* 85, no. 8 (2020): 2317–2328, https://doi.org/10.1111/1750-3841.15337.

21. P. Abdolsattari, S. H. Peighambardoust, S. Pirsa, S. J. Peighambardoust, and S. H. Fasihnia, "Investigating Microbial Properties of Traditional Iranian White Cheese Packed in Active LDPE Films Incorporating Metallic and Organoclay Nanoparticles," *Chemical Review and Letters* 3, no. 4 (2020): 168–174, https://doi.org/10.22034/CRL.2020.231587.1059.

22. S. H. Fasihnia, S. H. Peighambardoust, and S. J. Peighambardoust, "Nanocomposite Films Containing Organoclay Nanoparticles as an Antimicrobial (Active) Packaging for Potential Food Application," *Journal of Food Processing and Preservation* 42, no. 2 (2018): e13488, https://doi.org/10.1111/JFPP.13488.

23. A. Yousefi, S. Zinatloo-Ajabshir, M. Jekle, and M. Y. Panah, "Rapid and Green Combustion Synthesis of Dysprosium Cerium Oxide Nanostructures: Incorporation Into Wheat Starch/Sage Seed Gum Hybrid Composites," *International Journal of Biological Macromolecules* 308 (2025): 142502, https://doi.org/10.1016/J.IJBIOMAC.2025.142502.

24. F. Hossein Panahi, S. J. Peighambardoust, S. Davaran, and R. Salehi, "Development and Characterization of PLA-mPEG Copolymer Containing Iron Nanoparticle-Coated Carbon Nanotubes for Controlled Delivery of Docetaxel," *Polymer (Guildf)* 117 (2017): 117–131, https://doi.org/10.1016/J.POLYMER.2017.03.084.

25. S. Zinatloo-Ajabshir and M. Salavati-Niasari, "Preparation of Magnetically Retrievable CoFe2O4@SiO2@Dy2Ce2O7 Nanocomposites as Novel Photocatalyst for Highly Efficient Degradation of Organic Contaminants," *Composites Part B, Engineering* 174 (2019): 106930, https://doi.org/10.1016/J.COMPOSITESB.2019.106930.

26. H. Etemadi, S. Afsharkia, S. Zinatloo-Ajabshir, and E. Shokri, "Effect of Alumina Nanoparticles on the Antifouling Properties of Polycarbonate-Polyurethane Blend Ultrafiltration Membrane for Water Treatment," *Polymer Engineering and Science* 61, no. 9 (2021): 2364–2375, https://doi.org/10.1002/PEN.25764.

27. S. Zinatloo-Ajabshir, M. S. Morassaei, and M. Salavati-Niasari, "Eco-Friendly Synthesis of Nd2Sn2O7–Based Nanostructure Materials Using Grape Juice as Green Fuel as Photocatalyst for the Degradation of Erythrosine," *Composites Part B: Engineering* 167 (2019): 643–653, https://doi.org/10.1016/J.COMPOSITESB.2019.03.045.

28. M. Rezayeenik, M. Mousavi-Kamazani, and S. Zinatloo-Ajabshir, "CeVO4/rGO Nanocomposite: Facile Hydrothermal Synthesis, Characterization, and Electrochemical Hydrogen Storage," *Applied Physics A: Materials Science and Processing* 129, no. 1 (2023): 1–12, https://doi.org/10.1007/S00339-022-06325-Y/TABLES/2.

29. J. M. Raquez, Y. Habibi, M. Murariu, and P. Dubois, "Polylactide (PLA)-Based Nanocomposites," *Progress in Polymer Science* 38, no. 10–11 (2013): 1504–1542, https://doi.org/10.1016/J.PROGPOLYMSCI.2013.05.014.

30. A. Schneider Teixeira, L. Deladino, and N. Zaritzky, "Yerba Mate (*Ilex paraguariensis*) Waste and Alginate as a Matrix for the Encapsulation of N Fertilizer," *ACS Sustainable Chemistry & Engineering* 4, no. 4 (2016): 2449–2458, https://doi.org/10.1021/acssuschemeng.6b00344.

31. M. P. Arrieta, L. Peponi, D. López, and M. Fernández-García, "Recovery of Yerba Mate (*Ilex paraguariensis*) Residue for the Development of PLA-Based Bionanocomposite Films," *Industrial Crops and Products* 111 (2018): 317–328, https://doi.org/10.1016/J.INDCROP.2017.10.042.

32. F. R. Beltrán, M. P. Arrieta, G. Gaspar, M. U. de la Orden, and J. M. Urreaga, "Effect of Iignocellulosic Nanoparticles Extracted From Yerba Mate (*Ilex paraguariensis*) on the Structural, Thermal, Optical and Barrier Properties of Mechanically Recycled Poly(Lactic Acid)," *Polymers* 12, no. 8 (2020): 1690, https://doi.org/10.3390/POLYM12081690.

33. S. R. Lanjewar, P. S. Bari, D. P. Hansora, and S. Mishra, "Preparation and Analysis of Polypropylene Composites With Maleated Tea Dust Particles," *IEEE Journal of Selected Topics in Quantum Electronics* 25, no. 2 (2018): 373–381, https://doi.org/10.1515/secm-2015-0345.

34. J. Sempere-Torregrosa, J. M. Ferri, H. de la Rosa-Ramírez, C. Pavon, and M. D. Samper, "Effect of Epoxidized and Maleinized Corn Oil on Properties of Polylactic Acid (PLA) and Polyhydroxybutyrate (PHB) Blend," *Polymers (Basel)* 14, no. 19 (2022): 4205, https://doi.org/10.3390/polym14194205.

35. H. Han, L. Ke, H. Wang, et al., "Incidental Nanoparticles in Black Tea Infusion: Carriers of Bioactives Fortifying Protection on Intestinal Mucosal Cells Against Oxidative Stresses," *Food Biophysics* 17, no. 2 (2022): 209–220, https://doi.org/10.1007/S11483-021-09708-5.

36. L. Bartošová, M. Janalíková, J. Sedlaříková, et al., "Antibacterial and Biodegradable PLA-Based Nanofibers Loaded With Natural Phenolic Monoterpenes for Sustainable Biomedical or Food Application," *New Biotechnology* 87 (2025): 1–11, https://doi.org/10.1016/J.NBT.2025.02.005.

37. E. Malekzadeh, A. Tatari, and M. Dehghani Firouzabadi, "Effects of Biodegradation of Starch-Nanocellulose Films Incorporated With Black Tea Extract on Soil Quality," *Scientific Reports* 14, no. 1 (2024): 1–21, https://doi.org/10.1038/S41598-024-69841-2;SUBJMETA=166,172,45,47,631,639,704;KWRD=BIOCHEMISTRY,BIOGEOCHEMISTRY,ENGINEERING,ENVIRONMENTAL+SCIENCES.

38. E. Fortunati, F. Luzi, D. Puglia, and L. Torre, "Extraction of Lignocellulosic Materials From Waste Products," in *Multifunctional Polymeric Nanocomposites Based on Cellulosic Reinforcements* (William Andrew, 2016), 1–38, https://doi.org/10.1016/B978-0-323-44248-0.00001-8.

39. M. Kumar, R. K. Mishra, and A. K. Banthia, "Development of Pectin Based Hydrogel Membranes for Biomedical Applications," *International Journal of Plastics Technology* 14, no. 2 (2011): 213–223, https://doi.org/10.1007/S12588-011-0019-5.

40. G. Mondragon, S. Fernandes, A. Retegi, et al., "A Common Strategy to Extracting Cellulose Nanoentities From Different Plants," *Industrial Crops and Products* 55 (2014): 140–148, https://doi.org/10.1016/j.indcrop.2014.02.014.

41. E. Rayón, S. Ferrandiz, M. I. Rico, J. López, and M. P. Arrieta, "Microstructure, Mechanical, and Thermogravimetric Characterization of Cellulosic By-Products Obtained From Biomass Seeds," *International Journal of Food Properties* 18, no. 6 (2015): 1211–1222, https://doi.org/10.1080/10942912.2014.884578.

42. A. Valdés, O. Fenollar, A. Beltrán, et al., "Characterization and Enzymatic Degradation Study of Poly(ε-Caprolactone)-Based Biocomposites From Almond Agricultural By-Products," *Polymer Degradation and Stability* 132 (2016): 181–190, https://doi.org/10.1016/j.polymdegradstab.2016.02.023.

43. W. Yang, J. M. Kenny, and D. Puglia, "Structure and Properties of Biodegradable Wheat Gluten Bionanocomposites Containing Lignin Nanoparticles," *Industrial Crops and Products* 74 (2015): 348–356, https://doi.org/10.1016/j.indcrop.2015.05.032.

44. W. Yang, F. Dominici, E. Fortunati, J. M. Kenny, and D. Puglia, "Effect of Lignin Nanoparticles and Masterbatch Procedures on the Final Properties of Glycidyl Methacrylate-g-Poly (Lactic Acid) Films Before and After Accelerated UV Weathering," *Industrial Crops and Products* 77 (2015): 833–844, https://doi.org/10.1016/j.indcrop.2015.09.057.

45. K. Khalaf Hammud, A. Mohammed Raouf, A. Mohammed Ali Al-Sammarrie, and R. Raheem Neema, "New Chemically Prepared-Waste Cooked Tea Based Activated Carbon: FTIR, XRD, AFM, and Sem Spectroscopic Studies," *International Journal of Research in Pharmacy and Chemistry* 6, no. 2 (2016): 220–229, www.ijrpc.com.

46. M. C. A. Marcelo, D. Pozebon, and M. F. Ferrão, "Authentication of Yerba Mate According to the Country of Origin by Using Fourier Transform Infrared (FTIR) Associated With Chemometrics," *Food Additives & Contaminants. Part A, Chemistry, Analysis, Control, Exposure & Risk Assessment* 32, no. 8 (2015): 1215–1222, https://doi.org/10.1080/19440049.2015.1050702.

47. T. Zhao, Z. Chen, X. Lin, Z. Ren, B. Li, and Y. Zhang, "Preparation and Characterization of Microcrystalline Cellulose (MCC) From Tea Waste," *Carbohydrate Polymers* 184 (2018): 164–170, https://doi.org/10.1016/j.carbpol.2017.12.024.

48. S. Polat, E. Apaydın-Varol, and A. E. Pütün, "TGA-FTIR Study on the Thermal Decomposition of Tea Waste," 2013, https://www.researchgate.net/publication/337874141.

49. P. T. A. N. Kungel, V. G. Correa, R. C. G. Corrêa, et al., "Antioxidant and Antimicrobial Activities of a Purified Polysaccharide From Yerba Mate (*Ilex paraguariensis*)," *International Journal of Biological Macromolecules* 114 (2018): 1161–1167, https://doi.org/10.1016/J.IJBIOMAC.2018.04.020.

50. Y. Peng, Y. Wu, and Y. Li, "Development of Tea Extracts and Chitosan Composite Films for Active Packaging Materials," *International Journal of Biological Macromolecules* 59 (2013): 282–289, https://doi.org/10.1016/J.IJBIOMAC.2013.04.019.

51. S. Singh, C. Wu, and P. T. Williams, "Pyrolysis of Waste Materials Using TGA-MS and TGA-FTIR as Complementary Characterisation Techniques," *Journal of Analytical and Applied Pyrolysis* 94 (2012): 99–107, https://doi.org/10.1016/J.JAAP.2011.11.011.

52. M. P. Arrieta, M. M. Castro-López, E. Rayón, et al., "Plasticized Poly(Lactic Acid)-poly(Hydroxybutyrate) (PLA-PHB) Blends Incorporated With Catechin Intended for Active Food-Packaging Applications," *Journal of Agricultural and Food Chemistry* 62, no. 41 (2014): 10170–10180, https://doi.org/10.1021/JF5029812.

53. I. Armentano, E. Fortunati, N. Burgos, et al., "Processing and Characterization of Plasticized PLA/PHB Blends for Biodegradable Multiphase Systems," *Express Polymer Letters* 9, no. 7 (2015): 583–596, https://doi.org/10.3144/expresspolymlett.2015.55.

54. M. P. Arrieta, J. López, D. López, J. M. Kenny, and L. Peponi, "Effect of Chitosan and Catechin Addition on the Structural, Thermal, Mechanical and Disintegration Properties of Plasticized Electrospun PLA-PHB Biocomposites," *Polymer Degradation and Stability* 132 (2016): 145–156, https://doi.org/10.1016/j.polymdegradstab.2016.02.027.

55. M. L. Iglesias Montes, D. A. D'amico, L. B. Manfredi, and V. P. Cyras, "Effect of Natural Glyceryl Tributyrate as Plasticizer and Compatibilizer on the Performance of Bio-Based Polylactic Acid/Poly(3-Hydroxybutyrate) Blends," *Journal of Polymers and the Environment* 27, no. 7 (2019): 1429–1438, https://doi.org/10.1007/s10924-019-01425-y.

56. A. Lopera-Valle, J. V. Caputo, R. Leão, D. Sauvageau, S. M. Luz, and A. Elias, "Influence of Epoxidized Canola Oil (eCO) and Cellulose Nanocrystals (CNCs) on the Mechanical and Thermal Properties of Polyhydroxybutyrate (PHB)-poly(Lactic Acid) (PLA) Blends," *Polymers (Basel)* 11, no. 6 (2019): 933, https://doi.org/10.3390/polym11060933.

57. M. Ö. Seydibeyoğlu, M. Misra, and A. Mohanty, "Synergistic Improvements in the Impact Strength and % Elongation of Polyhydroxybutyrate-Co-Valerate Copolymers With Functionalized Soybean Oils and Poss," *International Journal of Plastics Technology* 14, no. 1 (2010): 1–16, https://doi.org/10.1007/S12588-010-0005-3/FIGURES/5.

58. I. Dominguez-Candela, J. Gomez-Caturla, S. C. Cardona, J. Lora-García, and V. Fombuena, "Novel Compatibilizers and Plasticizers Developed From Epoxidized and Maleinized Chia Oil in Composites Based on PLA and Chia Seed Flour," *European Polymer Journal* 173 (2022): 111289, https://doi.org/10.1016/j.eurpolymj.2022.111289.

59. S. Mazinani, R. Ramezani, S. Darvishmanesh, G. F. Molelekwa, R. Di Felice, and B. Van Der Bruggen, "A Ground Breaking Polymer Blend for CO2/N2 Separation," *Journal of CO2 Utilization* 27 (2018): 536–546, https://doi.org/10.1016/J.JCOU.2018.08.024.

60. S. Angelini, P. Cerruti, B. Immirzi, G. Santagata, G. Scarinzi, and M. Malinconico, "From Biowaste to Bioresource: Effect of a Lignocellulosic Filler on the Properties of Poly(3-Hydroxybutyrate)," *International Journal of Biological Macromolecules* 71 (2014): 163–173, https://doi.org/10.1016/J.IJBIOMAC.2014.07.038.

61. J. F. Balart, V. Fombuena, O. Fenollar, T. Boronat, and L. Sánchez-Nacher, "Processing and Characterization of High Environmental Efficiency Composites Based on PLA and Hazelnut Shell Flour (HSF) With Biobased Plasticizers Derived From Epoxidized Linseed Oil (ELO)," *Composites Part B: Engineering* 86 (2016): 168–177, https://doi.org/10.1016/J.COMPOSITESB.2015.09.063.

62. K. Madhavan Nampoothiri, N. R. Nair, and R. P. John, "An Overview of the Recent Developments in Polylactide (PLA) Research," *Bioresource Technology* 101, no. 22 (2010): 8493–8501, https://doi.org/10.1016/J.BIORTECH.2010.05.092.

63. E. Cavallo, X. He, F. Luzi, et al., "UV Protective, Antioxidant, Antibacterial and Compostable Polylactic Acid Composites Containing Pristine and Chemically Modified Lignin Nanoparticles," *Molecules* 26, no. 1 (2020): 126, https://doi.org/10.3390/MOLECULES26010126.

64. E. Fortunati, M. Gigli, F. Luzi, et al., "Processing and Characterization of Nanocomposite Based on Poly(Butylene/Triethylene Succinate) Copolymers and Cellulose Nanocrystals," *Carbohydrate Polymers* 165 (2017): 51–60, https://doi.org/10.1016/J.CARBPOL.2017.02.024.

65. A. Masek, S. Cichosz, and M. Piotrowska, "Biocomposites of Epoxidized Natural Rubber/Poly(Lactic Acid) Modified With Natural Fillers (Part I)," *International Journal of Molecular Sciences* 22, no. 6 (2021): 3150, https://doi.org/10.3390/IJMS22063150.

66. F. Pawlak, M. Aldas, J. López-Martínez, and M. D. Samper, "Effect of Different Compatibilizers on Injection-Molded Green Fiber-Reinforced Polymers Based on Poly(Lactic Acid)-Maleinized Linseed Oil System and Sheep Wool," *Polymers* 11, no. 9 (2019): 1514, https://doi.org/10.3390/POLYM11091514.

67. C. Medina Jaramillo, T. J. Gutiérrez, S. Goyanes, C. Bernal, and L. Famá, "Biodegradability and Plasticizing Effect of Yerba Mate Extract on Cassava Starch Edible Films," *Carbohydrate Polymers* 151 (2016): 150–159, https://doi.org/10.1016/j.carbpol.2016.05.025.

68. A. Iordanskii, A. Zhulkina, A. Olkhov, S. Fomin, A. Burkov, and M. Stilman, "Characterization and Evaluation of Controlled Antimicrobial Release From Petrochemical (PU) and Biodegradable (PHB) Packaging," *Polymers* 10, no. 8 (2018): 817, https://doi.org/10.3390/POLYM10080817.

69. A. L. Iordanskii, "Segmental Mobility in Crystalline Poly(3-Hydroxybutyrate) Studied by EPR Probe Technique," accessed June 27, 2024, https://www.researchgate.net/publication/280979673.

70. D. Garcia-Garcia, J. M. Ferri, N. Montanes, J. Lopez-Martinez, and R. Balart, "Plasticization Effects of Epoxidized Vegetable Oils on Mechanical Properties of Poly(3-Hydroxybutyrate)," *Polymer International* 65, no. 10 (2016): 1157–1164, https://doi.org/10.1002/PI.5164.

71. A. D'Anna, R. Arrigo, and A. Frache, "PLA/PHB Blends: Biocompatibilizer Effects," *Polymers* 11, no. 9 (2019): 1416, https://doi.org/10.3390/POLYM11091416.

72. J. M. Ferri, M. D. Samper, D. García-Sanoguera, M. J. Reig, O. Fenollar, and R. Balart, "Plasticizing Effect of Biobased Epoxidized Fatty Acid Esters on Mechanical and Thermal Properties of Poly(Lactic Acid)," *Journal of Materials Science* 51, no. 11 (2016): 5356–5366, https://doi.org/10.1007/s10853-016-9838-2.

73. B. W. Chieng, N. A. Ibrahim, Y. Y. Then, and Y. Y. Loo, "Epoxidized Vegetable Oils Plasticized Poly(Lactic Acid) Biocomposites: Mechanical, Thermal and Morphology Properties," *Molecules* 19, no. 10 (2014): 16024–16038, https://doi.org/10.3390/MOLECULES191016024.

74. A. J. Jose and M. Alagar, "Preparation and Characterization of Polysulfone-Based Nanocomposites," in *Manufacturing of Nanocomposites With Engineering Plastics* (Elsevier, 2015), 31–59, https://doi.org/10.1016/B978-1-78242-308-9.00003-3.

75. M. P. Arrieta, J. López, S. Ferrándiz, and M. A. Peltzer, "Characterization of PLA-Limonene Blends for Food Packaging Applications," *Polymer Testing* 32, no. 4 (2013): 760–768, https://doi.org/10.1016/J.POLYMERTESTING.2013.03.016.

76. C. Deng, Q. Tang, Z. Yang, et al., "Effects of Iron Oxide Nanoparticles on Phenotype and Metabolite Changes in Hemp Clones (*Cannabis sativa* L.)," *Frontiers of Environmental Science & Engineering* 16, no. 10 (2022): 134, https://doi.org/10.1007/s11783-022-1569-9.

77. Y. Han, Y. Weng, and C. Zhang, "Development of Biobased Plasticizers With Synergistic Effects of Plasticization, Thermal Stabilization, and Migration Resistance: A Review," *Journal of Vinyl and Additive Technology* 30, no. 1 (2024): 26–43, https://doi.org/10.1002/vnl.22048.

78. R. A. Ilyas, A. Azmi, N. M. Nurazzi, et al., "Oxygen Permeability Properties of Nanocellulose Reinforced Biopolymer Nanocomposites," *Materials Today: Proceedings* 52 (2021): 2414–2419, https://doi.org/10.1016/j.matpr.2021.10.420.

79. M. D. Sanchez-Garcia, E. Gimenez, and J. M. Lagaron, "Morphology and Barrier Properties of Nanobiocomposites of Poly(3-Hydroxybutyrate) and Layered Silicates," *Journal of Applied Polymer Science* 108, no. 5 (2008): 2787–2801, https://doi.org/10.1002/app.27622.

80. Z. Song, H. Xiao, and Y. Zhao, "Hydrophobic-Modified Nano-Cellulose Fiber/PLA Biodegradable Composites for Lowering Water Vapor Transmission Rate (WVTR) of Paper," *Carbohydrate Polymers* 111 (2014): 442–448, https://doi.org/10.1016/J.CARBPOL.2014.04.049.

81. N. Bumbudsanpharoke, N. Harnkarnsujarit, B. Chongcharoenyanon, S. Kwon, and S. Ko, "Enhanced Properties of PBAT/TPS Biopolymer Blend With CuO Nanoparticles for Promising Active Packaging," *Food Packaging and Shelf Life* 37 (2023): 101072, https://doi.org/10.1016/J.FPSL.2023.101072.

82. R. Auras, B. Harte, and S. Selke, "An Overview of Polylactides as Packaging Materials," *Macromolecular Bioscience* 16 (2004): 835–864, https://doi.org/10.1002/mabi.200400043.

83. E. Fortunati, I. Armentano, A. Iannoni, et al., "New Multifunctional Poly(Lactide Acid) Composites: Mechanical, Antibacterial, and Degradation Properties," *Journal of Applied Polymer Science* 124, no. 1 (2012): 87–98, https://doi.org/10.1002/app.35039.

84. V. Siracusa, I. Blanco, S. Romani, U. Tylewicz, P. Rocculi, and M. D. Rosa, "Poly(Lactic Acid)-Modified Films for Food Packaging Application: Physical, Mechanical, and Barrier Behavior," *Journal of Applied Polymer Science* 125, no. Suppl. 2 (2012): E390–E401, https://doi.org/10.1002/app.36829.

85. E. Fortunati, D. Puglia, C. Santulli, F. Sarasini, and J. M. Kenny, "Biodegradation of *Phormium tenax*/Poly(Lactic Acid) Composites," *Journal of Applied Polymer Science* 125, no. S2 (2012): E562–E572, https://doi.org/10.1002/APP.36839.

86. L. Guo, H. Sato, T. Hashimoto, and Y. Ozaki, "FTIR Study on Hydrogen-Bonding Interactions in Biodegradable Polymer Blends of Poly(3-Hydroxybutyrate) and Poly(4-Vinylphenol)," *Macromolecules* 43, no. 8 (2010): 3897–3902, https://doi.org/10.1021/MA100307M.

87. T. Furukawa, H. Sato, R. Murakami, et al., "Structure, Dispersibility, and Crystallinity of Poly(Hydroxybutyrate)/Poly(L-Lactic Acid) Blends Studied by FT-IR Microspectroscopy and Differential Scanning Calorimetry," *Macromolecules* 38, no. 15 (2005): 6445–6454, https://doi.org/10.1021/ma0504668.

88. P. S. D. O. Patrício, F. V. Pereira, M. C. Dos Santos, P. P. De Souza, J. P. B. Roa, and R. L. Orefice, "Increasing the Elongation at Break of Polyhydroxybutyrate Biopolymer: Effect of Cellulose Nanowhiskers on Mechanical and Thermal Properties," *Journal of Applied Polymer Science* 127, no. 5 (2013): 3613–3621, https://doi.org/10.1002/APP.37811.

89. A. I. Romero, J. M. Bermudez, M. Villegas, M. F. Dib Ashur, M. L. Parentis, and E. E. Gonzo, "Modeling of Progesterone Release From Poly(3-Hydroxybutyrate) (PHB) Membranes," *AAPS PharmSciTech* 17, no. 4 (2016): 898–906, https://doi.org/10.1208/S12249-015-0410-1/FIGURES/7.

90. A. Leonés, V. Salaris, L. Peponi, et al., "Bioactivity and Antibacterial Analysis of Plasticized PLA Electrospun Fibers Reinforced With MgO and Mg(OH)2 Nanoparticles," *Polymers* 16, no. 12 (2024): 1727, https://doi.org/10.3390/POLYM16121727.

91. M. L. Iglesias-Montes, M. Soccio, V. Siracusa, et al., "Chitin Nanocomposite Based on Plasticized Poly(Lactic Acid)/poly(3-Hydroxybutyrate) (PLA/PHB) Blends as Fully Biodegradable Packaging Materials," *Polymers* 14, no. 15 (2022): 3177, https://doi.org/10.3390/POLYM14153177.

92. D. Li, Y. Jiang, S. Lv, et al., "Preparation of Plasticized Poly (Lactic Acid) and Its Influence on the Properties of Composite Materials," *PLoS One* 13, no. 3 (2018): e0193520, https://doi.org/10.1371/JOURNAL.PONE.0193520.

93. M. Carrasco-Fernández, E. I. López-Martínez, S. G. Flores-Gallardo, I. A. Estrada-Moreno, M. E. Mendoza-Duarte, and A. Vega-Rios, "Innovative Poly(Lactic Acid) Blends: Exploring the Impact of the Diverse Chemical Architectures From Itaconic Acid," *Polymers (Basel)* 16, no. 19 (2024): 2780, https://doi.org/10.3390/POLYM16192780/S1.

94. Á. Agüero, E. Corral Perianes, S. S. Abarca de las Muelas, et al., "Plasticized Mechanical Recycled PLA Films Reinforced With Microbial Cellulose Particles Obtained From Kombucha Fermented in Yerba Mate Waste," *Polymers* 15, no. 2 (2023): 285, https://doi.org/10.3390/POLYM15020285.

95. M. P. Arrieta, E. Fortunati, F. Dominici, J. López, and J. M. Kenny, "Bionanocomposite Films Based on Plasticized PLA–PHB/Cellulose Nanocrystal Blends," *Carbohydrate Polymers* 121 (2015): 265–275, https://doi.org/10.1016/J.CARBPOL.2014.12.056.

96. M. P. Arrieta, E. Fortunati, F. Dominici, E. Rayón, J. López, and J. M. Kenny, "PLA-PHB/Cellulose Based Films: Mechanical, Barrier and Disintegration Properties," *Polymer Degradation and Stability* 107 (2014): 139–149, https://doi.org/10.1016/J.POLYMDEGRADSTAB.2014.05.010.

97. H. de la Rosa-Ramírez, M. Aldas, J. M. Ferri, F. Pawlak, J. López-Martínez, and M. D. Samper, "Control of Biodegradability Under Composting Conditions and Physical Performance of Poly (Lactic Acid) Based Materials Modified With Phenolic-Free Rosin Resin," *Journal of*

*Polymers and the Environment* 31, no. 12 (2023): 5462–5476, https://doi.org/10.1007/S10924-023-02956-1/FIGURES/9.

98. Y. Chen, L. Zeng, Y. Liao, et al., "Enzymatic Reaction-Related Protein Degradation and Proteinaceous Amino Acid Metabolism During the Black Tea (*Camellia sinensis*) Manufacturing Process," *Food* 9, no. 1 (2020): 66, https://doi.org/10.3390/FOODS9010066.

99. A. Gawron-Gzella, J. Chanaj-Kaczmarek, and J. Cielecka-Piontek, "Yerba Mate—A Long but Current History," *Nutrients* 13, no. 11 (2021): 3706, https://doi.org/10.3390/NU13113706.